Journal of Virology

Host-Microbial Interactions | Full-Length Text

EGR1 functions as a new host restriction factor for SARS-CoV-2 to inhibit virus replication through the E3 ubiquitin ligase MARCH8

Yinghua Zhao,[1,2] Liyan Sui,[1] Ping Wu,[2] Letian Li,[3] Li Liu,[2] Baohua Ma,[2] Wenfang Wang,[4] Hongmiao Chi,[4] Ze-Dong Wang,[1] Zhengkai Wei,[5] Zhijun Hou,[2] Kaiyu Zhang,[1] Junqi Niu,[1] Ningyi Jin,[3] Chang Li,[3] Jixue Zhao,[6] Guoqing Wang,[4] Quan Liu[1,2,5,7]

AUTHOR AFFILIATIONS See affiliation list on p. 18.

ABSTRACT Coronavirus disease 2019, caused by severe acute respiratory syndrome coronavirus 2 (SARS-CoV-2), has led to an unprecedented public health crisis worldwide. Though the host produces interferons (IFNs) and restriction factors to suppress virus infection, SARS-CoV-2 has evolved multiple strategies to inhibit the antiviral responses. Understanding host restriction factors and viral escape mechanisms is conducive to developing effective anti-SARS-CoV-2 drugs. Here, we constructed SARS-CoV-2 nucleocapsid (2N) protein- and green fluorescent protein (GFP)-stably expressing cells that were transfected with polyinosinic-polycytidylic acid (poly(I:C)) to activate IFN responses. The transcriptome analysis showed that poly(I:C)-induced IFN responses were inhibited by the SARS-CoV-2 N protein. Further analysis revealed that 2N inhibited the production of IFN-stimulated genes by suppressing early growth response gene-1 (EGR1) expression, a transcription factor that can regulate multiple cellular processes. The ectopic expression of EGR1 remarkably reduced 2N expression and suppressed SARS-CoV-2 replication. Mechanistically, EGR1 promoted expression of IFN-regulated antiviral protein (IRAV), which interacted with 2N to induce its degradation via the E3 ubiquitin ligase MARCH8 with the cargo receptor NDP52 in a lysosome-dependent pathway. MARCH8 catalyzed the K48-linked polyubiquitination of 2N at the lysine residue 143, and knockout of endogenous MARCH8 reversed IRAV-mediated 2N degradation. Additionally, the overexpression of IRAV or MARCH8 could inhibit SARS-CoV-2 replication. Our findings reveal that EGR1 is a new host restriction factor to inhibit SARS-CoV-2 replication through the E3 ubiquitin ligase MARCH8, which would contribute to understanding the pathogenesis of emerging coronaviruses.

IMPORTANCE Emerging vaccine-breakthrough severe acute respiratory syndrome coronavirus 2 (SARS-CoV-2) variants highlight an urgent need for novel antiviral therapies. Understanding the pathogenesis of coronaviruses is critical for developing antiviral drugs. Here, we demonstrate that the SARS-CoV-2 N protein suppresses interferon (IFN) responses by reducing early growth response gene-1 (EGR1) expression. The overexpression of EGR1 inhibits SARS-CoV-2 replication by promoting IFN-regulated antiviral protein expression, which interacts with and degrades SARS-CoV-2 N protein via the E3 ubiquitin ligase MARCH8 and the cargo receptor NDP52. The MARCH8 mutants without ubiquitin ligase activity are no longer able to degrade SARS-CoV-2 N proteins, indicating that MARCH8 degrades SARS-CoV-2 N proteins dependent on its ubiquitin ligase activity. This study found a novel immune evasion mechanism of SARS-CoV-2 utilized by the N protein, which is helpful for understanding the pathogenesis of SARS-CoV-2 and guiding the design of new prevention strategies against the emerging coronaviruses.

KEYWORDS SARS-CoV-2, nucleocapsid protein, interferon, EGR1, IFN-regulated antiviral protein, MARCH8

Editor Kanta Subbarao, The Peter Doherty Institute for Infection and Immunity, Melbourne, Victoria, Australia

Address correspondence to Jixue Zhao, jixue@jlu.edu.cn, Guoqing Wang, qing@jlu.edu.cn, or Quan Liu, liuquan1973@hotmail.com.

The authors declare no conflict of interest.

See the funding table on p. 18.

Received 11 July 2023
Accepted 13 August 2023
Published 29 September 2023

The coronavirus disease 2019 (COVID-19) pandemic, caused by severe acute respiratory syndrome coronavirus-2 (SARS-CoV-2), has spread globally, resulting in approximately 664 million infections and 6 million deaths (https://covid19.who.int/). The disease outcomes range from asymptomatic, mild courses to more severe and critical cases (1). Host antiviral immunity responses can promote virus clearance, but severe COVID-19 patients are characterized by an inefficient immune response that fails to suppress infection (2). Understanding host antiviral restriction factors and viral antagonists against innate immunity is conducive to developing effective anti-SARS-CoV-2 drugs.

Viruses depend on their ability to inhibit host cellular restriction factors and immune responses for successful replication (3–5). Following viral infection, the host pattern recognition receptors recognize viral RNAs of SARS-CoV-2 and rapidly activate the innate immune response, especially interferon pathways, to induce the expression of restriction factors such as interferon-stimulating genes (ISGs), ultimately suppressing virus replication (6, 7). In turn, SARS-CoV-2 has evolved multiple strategies to antagonize the interferon (IFN) system (1). The SARS-CoV-2 genome encodes 16 non-structural proteins (nsp1-16), 4 structural proteins (E, M, N, and S), and 9 accessory proteins (ORF3a, 3b, 6, 7a, 7b, 8, 9b, 9c, and 10), in which several viral proteins can antagonize host immune responses. The structural N protein promotes viral replication by regulating host-pathogen interactions and immune responses (8, 9), such as binding to stress granule proteins G3BP1, G3BP2, and HSPA1A involved in host RNA processing and regulation (10, 11), and interfering with TRIM25 to suppress type I interferon (IFN-I) production (12).

Early growth response gene-1 (EGR1), a zinc finger DNA-binding protein, is an important transcription factor associated with multiple cellular processes, including cell proliferation, survival, differentiation, and apoptosis (13, 14). EGR1 plays various roles in different viral infections. For example, EGR1 can facilitate human cytomegalovirus and Venezuelan equine encephalitis virus replication by promoting viral latent gene expression or host cell apoptosis (15, 16), whereas it can suppress foot-and-mouth disease virus and porcine epidemic diarrhea virus (PEDV) infection by activating IFN responses (17, 18). In this study, we found that SARS-CoV-2 N protein suppressed IFN responses by reducing EGR1 expression and overexpression of EGR1 inhibited SARS-CoV-2 replication by promoting IFN-regulated antiviral protein (IRAV) expression, which interacts with and degrades SARS-CoV-2 N protein via the E3 ubiquitin ligase MARCH8. The MARCH8-degraded SARS-CoV-2 N (2N) protein is dependent on its ubiquitin ligase activity. These findings would contribute to further understanding the pathogenesis of the emerging coronaviruses.

RESULTS

SARS-CoV-2 N protein inhibits IFN responses in 2N-stably expressing cells

SARS-CoV is most genetically related to SARS-CoV-2, sharing similar structure and pathogenicity (19), so we constructed SARS-CoV N- and SARS-CoV-2 N-stably expressing HEK293T cell lines to explore their roles in the regulation of IFN responses. The N- and green fluorescent protein (GFP)-stably expressing cells were transfected with or without polyinosinic-polycytidylic acid (Poly(I:C)) to activate IFN responses, and RNA-seq analysis (n = 3) was conducted at 24 h post transfection (hpt). The multivariate principal component (PCA) analysis showed good intra-group repeatability and inter-group variability (Fig. 1A). We determined the potential biological functions of differentially expressed genes (DEGs) in N proteins compared to the controls and identified the top 40 enriched Gene Ontology (GO) pathways (Fig. 1B). The GO analysis showed that the 2N protein regulated the organ development pathways to a greater extent than the N protein, such as in the ear, kidney, and midgut (Fig. 1B, triangle). The nervous system-associated pathways were also enriched, especially the abnormal development of the olfactory bulb and olfactory lobe, which may explain the anosmia of COVID-19 patients (Fig. 1B, star). In addition, IFN-I signaling was more obviously regulated by both N proteins upon poly(I:C) stimulation (Fig. 1B, diamond).

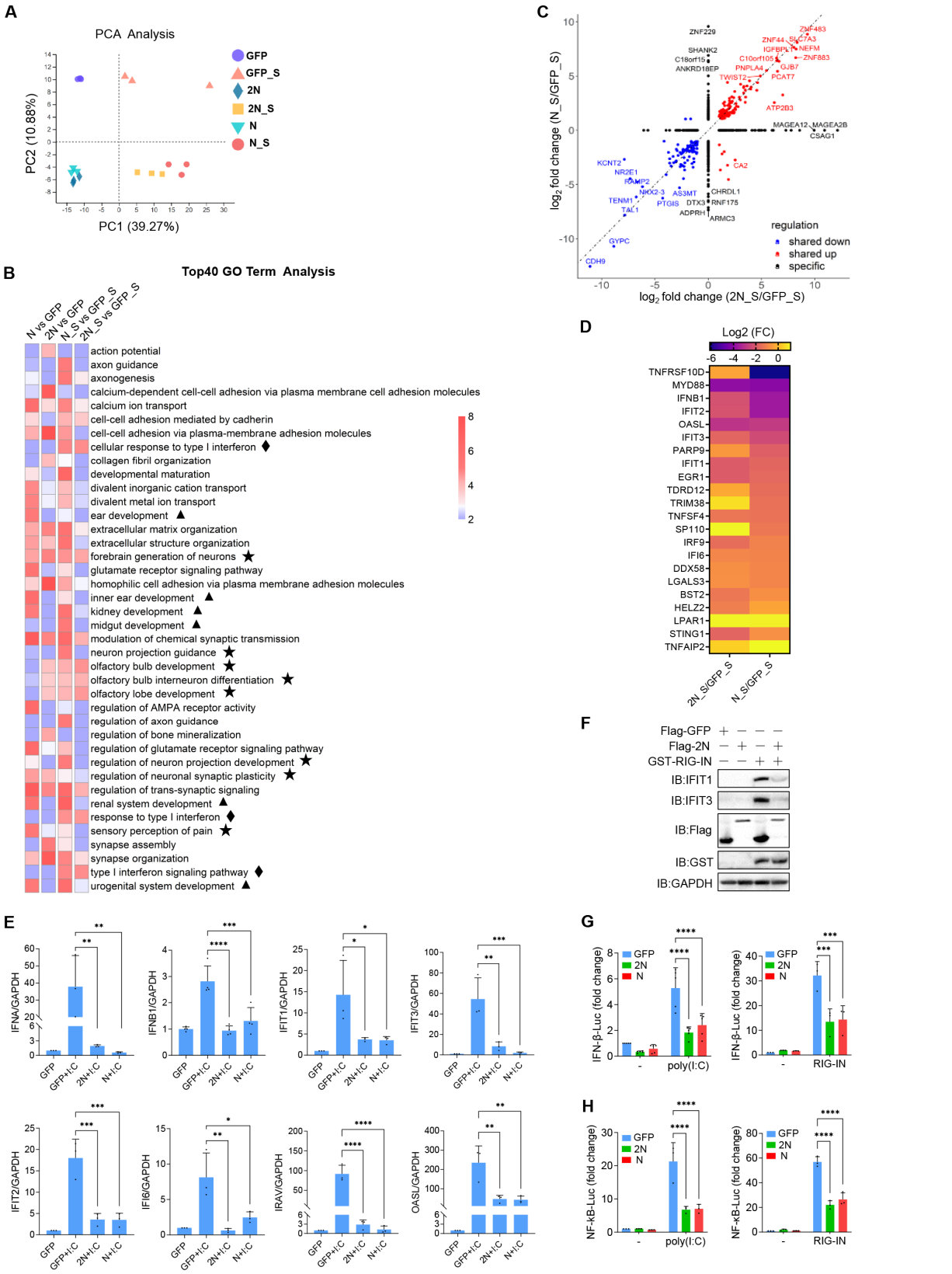

FIG 1 The SARS-CoV-2 N protein inhibits IFN responses in stable-expressing cells. (A–D) N protein- and GFP-stably expressing cells were stimulated with or without poly(I:C) to activate interferon responses. At 24 hpt, cells were analyzed by RNA-seq (n = 3). GPF/2 N/N were the stably expressing cells without poly(I:C) stimulation, and GPF_S /2N_S /N_S were the cells with poly(I:C) stimulation. (A) The PCA analysis of the RNA-seq. (B) Illustration of the enrichment *P*-values for

(Continued on next page)

FIG 1 (Continued)

selected GO pathways. The −log10 (*P*-values) are shown as a heat map. Triangle: organ development-related pathways; star: neuron-related pathways; diamond: type I IFN pathways. (C) Scatter plot for DEGs between 2N_S (x-axis) and N_S (y-axis) (log_2 fold change in comparison with GFP_S control). (D) The heatmap of IFN-I signaling-related DEGs for 2N_S and N_S compared to GFP_S by log_2 fold change. The color scale is shown at the top of the heatmap. (E) N proteins and GFP stable-expressing cells were transfected with or without poly(I:C). At 24 hpt, the mRNA levels of the indicated genes were examined using qPCR. (F) N and GFP stable-expressing cells were transfected with or without the RIG-IN plasmid. At 24 hpt, the protein expression of IFIT1, IFIT3, 2N, and RIG-IN was detected by immunoblots. (G and H) N and GFP stable-expressing cells were co-transfected with the IFN-β (G) or NF-κB (H) promoters and the control plasmid pGL4.74 and transfected with or without poly(I:C) (left) or RIG-IN (right). At 24 hpt, cells were harvested, and the luciferase activity was measured. One-way analysis of variance with multiple comparison correction was performed (*$P < 0.05$, **$P < 0.01$, ***$P < 0.001$, and ****$P < 0.0001$).

Next, we focused on the transcriptome of poly(I:C)-induced samples and found that the commonly upregulated genes by the N proteins included insulin-like growth factor binding protein like 1, zinc finger protein 44 (ZNF44), and ZNF483 (Fig. 1C; Tables S1 and S2), which are also increased upon both SARS-CoV and SARS-CoV-2 infection (10). We also found that almost all DEGs involved in the IFN-I pathway were reduced, such as the pattern recognition receptors *DDX58* and *MYD88*, the transcription factors *IRF9* and *EGR1*, the cytokine *IFNB1*, and ISGs (Fig. 1D). We then confirmed that both N proteins reduced poly(I:C)-induced mRNA expression of *IFNA*, *IFNB1*, *IRAV*, *IFIT1*, *IFIT2*, *IFIT3*, *IFI6*, and *OASL* using quantitative real-time PCR (qPCR) (Fig. 1E) and reduced RIG-IN (the constitutively active N-terminal domains of RIG-I)-induced protein expression of IFIT1 and IFIT3 using immunoblots (Fig. 1F). The dual luciferase reporter assays also showed that both N proteins significantly inhibited the promoter activity of IFN-β and NF-κB induced by poly(I:C) or RIG-IN (Fig. 1G and H), indicating that the SARS-CoV-2 N protein inhibited IFN-I responses in 2N stable-expressing cells. These results demonstrated that SARS-CoV-2 N protein inhibited the IFN-I responses in stably expressing cells, which was also seen in SARS-CoV N protein.

SARS-CoV-2 N protein reduces EGR1 expression to inhibit IFN-I responses

To clarify the mechanism by which N proteins inhibit IFN responses, we analyzed the differentially expressed transcription factors and found that the expression of zinc finger proteins was increased, whereas the expression of basic leucine zipper ATF-like transcription factor 2 (BATF2), interferon regulatory factor 9 (IRF9), and EGR1 was reduced by both N proteins (Fig. 2A). We then confirmed the changes in the mRNA levels for *BATF2*, *IRF9*, *EGR1*, and *ZNF738* using qPCR (Fig. 2B) and the protein levels for EGR1 and IRF9 via immunoblots (Fig. 2C). Both N proteins inhibited poly(I:C)-induced phosphorylation of STAT2, which is a pivotal transcription factor to elicit effective antiviral responses (Fig. 2C). Moreover, we found that 2N protein inhibited endogenous EGR1 expression in a dose-dependent manner (Fig. 2D). EGR1 is reported to be rapidly induced by IFN-α, IFN-β, and IFN-γ in human or mouse fibroblasts and acts as a transcription factor to drive expression of ISGs (18, 20, 21). Furthermore, we found that EGR1 overexpression partially reversed the inhibitory effect of both N proteins on the IFN-induced expression of ISGs (Fig. 2E), indicating that the SARS-CoV-2 N protein inhibited IFN-induced antiviral responses through reducing expression of EGR1.

EGR1 reduces SARS-CoV-2 N expression by promoting IRAV expression

EGR1 has recently been identified as a host restriction factor that suppresses PEDV replication by degrading the viral nucleocapsid protein (17). We have found that the expression of SARS-CoV-2 N protein was reduced by poly(I:C)-induced IFN responses (Fig. 3A), with an unknown mechanism. Thus, we sought to explore whether EGR1 is responsible for the reduction of 2N protein. HEK293T- or N protein-stably expressing cells were transfected with or without the EGR1 plasmid. The immunoblotting results revealed that overexpression of EGR1 reduced both N protein levels in cells that transiently or stably expressed N proteins (Fig. 3B through D). Moreover, knockout of endogenous EGR1 with small guide RNA (sgRNA) considerably increased the expression of 2N protein (Fig. 3E),

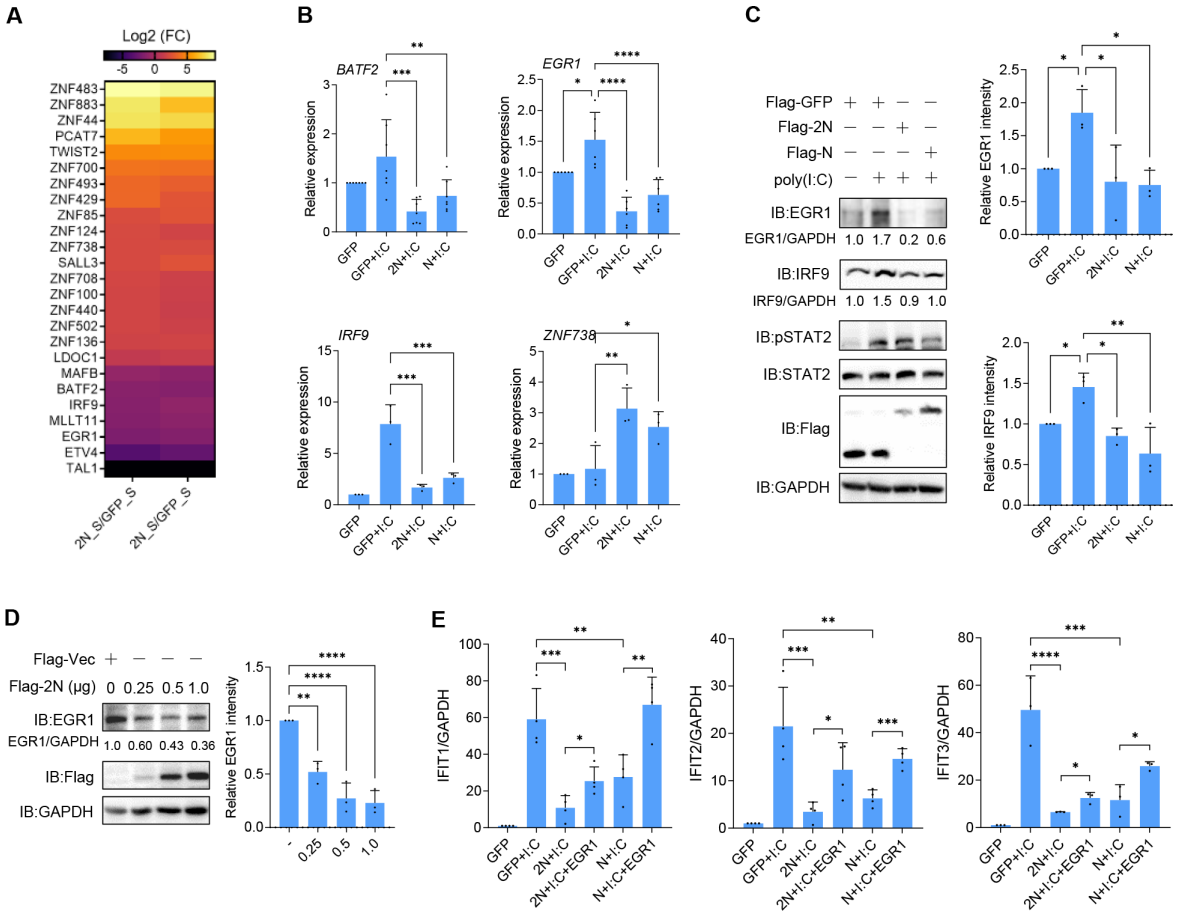

FIG 2 SARS-CoV-2 N protein reduces EGR1 expression to inhibit IFN-I responses. (A) The heatmap of the differentially expressed transcription factors for 2N_S and N_S compared to GFP_S. (B) N proteins and GFP stable-expressing cells were transfected with or without poly(I:C). At 24 hpt, the mRNA levels of *BATF2*, *EGR1*, *IRF9*, and *ZNF738* were examined using qPCR. GAPDH was used as an internal reference control. (C) HEK293T cells were transfected with N proteins or GFP plasmids, incubated for 24 h, and treated with or without poly(I:C) for another 16 h. The cell lysates were analyzed through immunoblotting. The gray-scale statistical analysis of EGR1 and IRF9 was displayed (right). (D) HEK293T cells were transfected with the dose-escalated 2N plasmids. After 24 h, cells were lysed and detected by immunoblotting. The gray-scale statistical analysis of EGR1 were displayed (right). (E) N proteins and GFP stable-expressing cells were transfected with or without poly(I:C) and EGR1. At 24 hpt, the mRNA levels of *IFIT1*, *IFIT2*, and *IFIT3* were examined using qPCR. One-way analysis of variance with multiple comparison correction was performed (**P* < 0.05, ***P* < 0.01, ****P* < 0.001, and *****P* < 0.0001).

demonstrating that EGR1 was responsible for inhibiting the expression of 2N protein. To explore whether EGR1 inhibits SARS-CoV-2 replication, Caco-2 cells that expressed exogenous EGR1 were infected with SARS-CoV-2. After 24 h, the viral replication levels were detected using qPCR, tissue culture median infectious dose ($TCID_{50}$), and immunoblotting, showing that EGR1 effectively inhibited SARS-CoV-2 replication (Fig. 3F through H). These data demonstrated that the ability of EGR1 to reduce expression of 2N correlates with its ability to inhibit replication of SARS-CoV-2 and EGR1 is a new host restriction factor for SARS-CoV-2.

EGR1 degrades PEDV N protein by promoting IRAV expression (17), and IRAV was reduced by SARS-CoV-2 N protein (Fig. 1E), so we speculate that EGR1 may inhibit SARS-CoV-2 replication through IRAV. HEK293T cells were transfected with a dose-escalated EGR1 plasmid. After 24 h, the expression of IRAV was measured using qPCR and immunoblotting, showing that EGR1 indeed promoted the expression of IRAV (Fig. 3I). To explore whether IRAV degrades 2N protein, HEK293T cells were co-transfected with 2N and dose-escalated IRAV plasmids and lysed for immunoblots, demonstrating that IRAV inhibited expression of 2N protein in a dose-dependent manner (Fig. 3J). In addition, we found that 2N protein dose-dependently reduced expression of IRAV (Fig. 3K) and

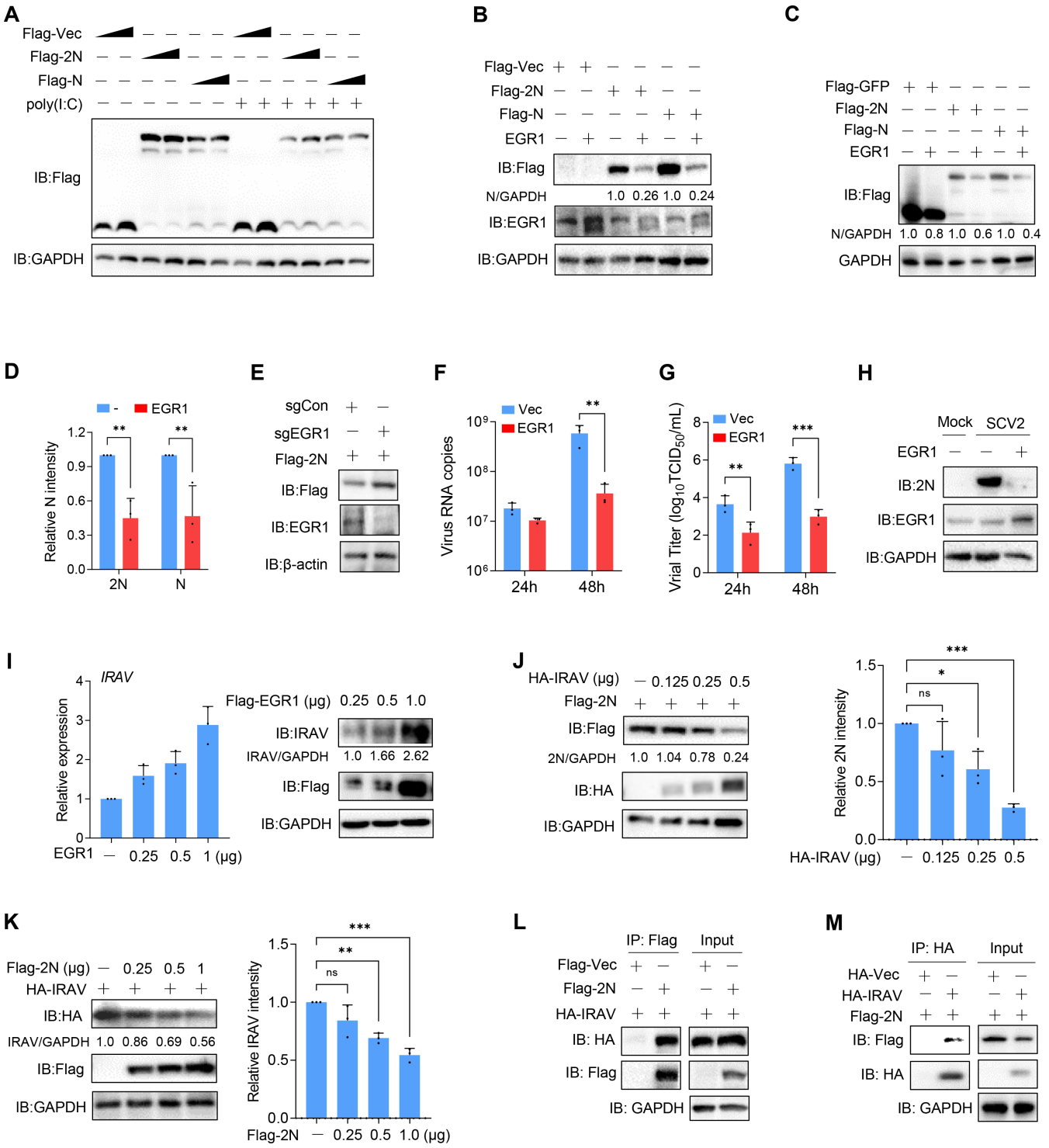

FIG 3 EGR1 promotes IRAV expression to inhibit SARS-CoV-2 N expression. (A) HEK293T cells were transfected with the dose-escalated 2N, N, or vector plasmids, incubated for 24 h, and treated with or without poly(I:C) for another 16 h. The cell lysates were analyzed through immunoblots. (B) HEK293T cells were co-transfected with the indicated plasmids. After 24 h, cells were lysed for immunoblots with anti-Flag and EGR1 antibodies. (C) N proteins and GFP stable-expressing cells were transfected with or without the EGR1 plasmid. After 24 h, cell lysates were analyzed through immunoblots. (D) The gray-scale statistical analysis of N proteins in (B) and (C). (E) HEK293T cells transfected with sgEGR1 or sgControl plasmids were cultured for 48 h, transfected with 2N plasmid, and incubated for another 24 h. Cell lysates were analyzed by immunoblots. (F–H) Caco-2 cells were transfected with EGR1 or vector plasmids. Twenty-four hours later, the cells were infected with SARS-CoV-2 at an MOI of 0.01. At 24 and 48 hpi, the viral RNA copies in supernatants were examined using qPCR (F); the viral titers were determined using $TCID_{50}$ assays (G); and the 2N and MARCH8 protein levels of cells were detected by immunoblots (H). (I) HEK293T

(Continued on next page)

FIG 3 (Continued)

cells were transfected with the dose-escalated EGR1 plasmid. After 24 hpt, the expression of IRAV was measured using qPCR (left) or immunoblots (right). (J) HEK293T cells were co-transfected with 2N and dose-escalated IRAV plasmids. After 24 h, cells were lysed for immunoblots. The gray-scale statistical analysis of 2N was displayed (right). (K) HEK293T cells were co-transfected with IRAV and dose-escalated 2N plasmids. Cells were lysed at 24 hpt and analyzed by immunoblots. The gray-scale statistical analysis of IRAV was displayed (right). (L and M) HEK293T cells were co-transfected with Flag-2N and HA-IRAV plasmids as indicated. At 48 hpt, co-IP was performed using the anti-Flag beads (L) or anti-HA beads (M), and the immunocomplexes were analyzed by immunoblots. A two-way analysis of variance with multiple comparison correction was performed (*$P < 0.05$, **$P < 0.01$, and ***$P < 0.001$).

interacted with IRAV (Fig. 3L and M). Collectively, these data indicated that EGR1 reduced the expression of the SARS-CoV-2 N protein by inducing IRAV expression.

IRAV promotes SARS-CoV-2 N degradation through MARCH8

MARCH8, a member of the MARCH E3 ubiquitin ligase family, not only degrades host transmembrane proteins to regulate cellular homeostasis but also acts as an antiviral factor to reduce viral glycoprotein expression through ubiquitination-dependent or tyrosine motif-dependent pathways (22–25). To explore the mechanism by which IRAV inhibits 2N protein expression, HEK293T cells were co-transfected with different combinations of 2N, MARCH8, and IRAV plasmids. At 48 h after transfection, coimmunoprecipitation (co-IP) results showed that 2N protein not only interacted with exogenous MARCH8 (Fig. 4A through C) but also inhibited IRAV and MARCH8 expression (Fig. 4A, input). We then confirmed that 2N protein interacted with endogenous IRAV and MARCH8 (Fig. 4D), indicating that 2N protein formed a complex with IRAV and MARCH8. We then validated the interaction between 2N and IRAV or MARCH8 via a microscale thermophoresis (MST) assay, which can measure binding affinities of binder-ligand systems based on the directional movement of molecules in a temperature gradient (26). The results showed that the binding affinity of 2N to IRAV was 40.926 µmol/L (Fig. 4E) and to MARCH8 was 118.4 µmol/L (Fig. 4F), indicating that 2N protein could directly bind to IRAV and MARCH8 with a moderate affinity *in vitro*.

To evaluate whether IRAV is involved in regulating MARCH8 expression, HEK293T cells were transfected with the IRAV plasmid. The immunoblotting and qPCR results showed that the mRNA and protein levels of MARCH8 were not affected by IRAV (Fig. 4G). To confirm the role of MARCH8 during IRAV-mediated 2N degradation, HEK293T cells treated with sgRNA targeting MARCH8 were transfected with 2N and IRAV plasmids. We found that the knockout of MARCH8 eliminated the inhibitory effect of IRAV on 2N expression (Fig. 4H), indicating that MARCH8 is responsible for IRAV-mediated 2N degradation. Additionally, the ectopic expression of MARCH8 reduced 2N protein levels (Fig. 4I and J), and the deficiency of MARCH8 reversed 2N protein degradation (Fig. 4K). The mutants of MARCH8^{W114A} and MARCH8$^{I82A/W114A}$ that abolish its interaction with E2 ubiquitin-conjugating enzyme (23) could not degrade 2N protein (Fig. 4L), indicating that MARCH8 degraded 2N protein dependent on its ubiquitin ligase activity. Overall, these findings demonstrated that IRAV promotes SARS-CoV-2 N protein degradation through the E3 ubiquitin ligase MARCH8.

MARCH8 degrades the SARS-CoV-2 N protein in a lysosome-dependent pathway

To explore the pathway by which 2N protein is degraded, HEK293T cells were co-transfected with 2N and EGR1 plasmids, followed by treatment with dimethyl sulfoxide (DMSO), proteasome inhibitor MG132, or lysosome inhibitor chloroquine (CQ). The immunoblotting results showed that CQ reversed EGR1-induced 2N protein reduction (Fig. 5A), indicating that EGR1 reduced 2N protein expression through a lysosomal pathway. Moreover, the lysosome inhibitors CQ and bafilomycin A1 (BafA1) reversed MARCH8-mediated 2N protein degradation (Fig. 5B), showing that MARCH8 also degraded 2N protein in a lysosome-dependent pathway. Immunofluorescence revealed that 2N was co-localized with lysosome marker LAMP-1, and accumulated in the

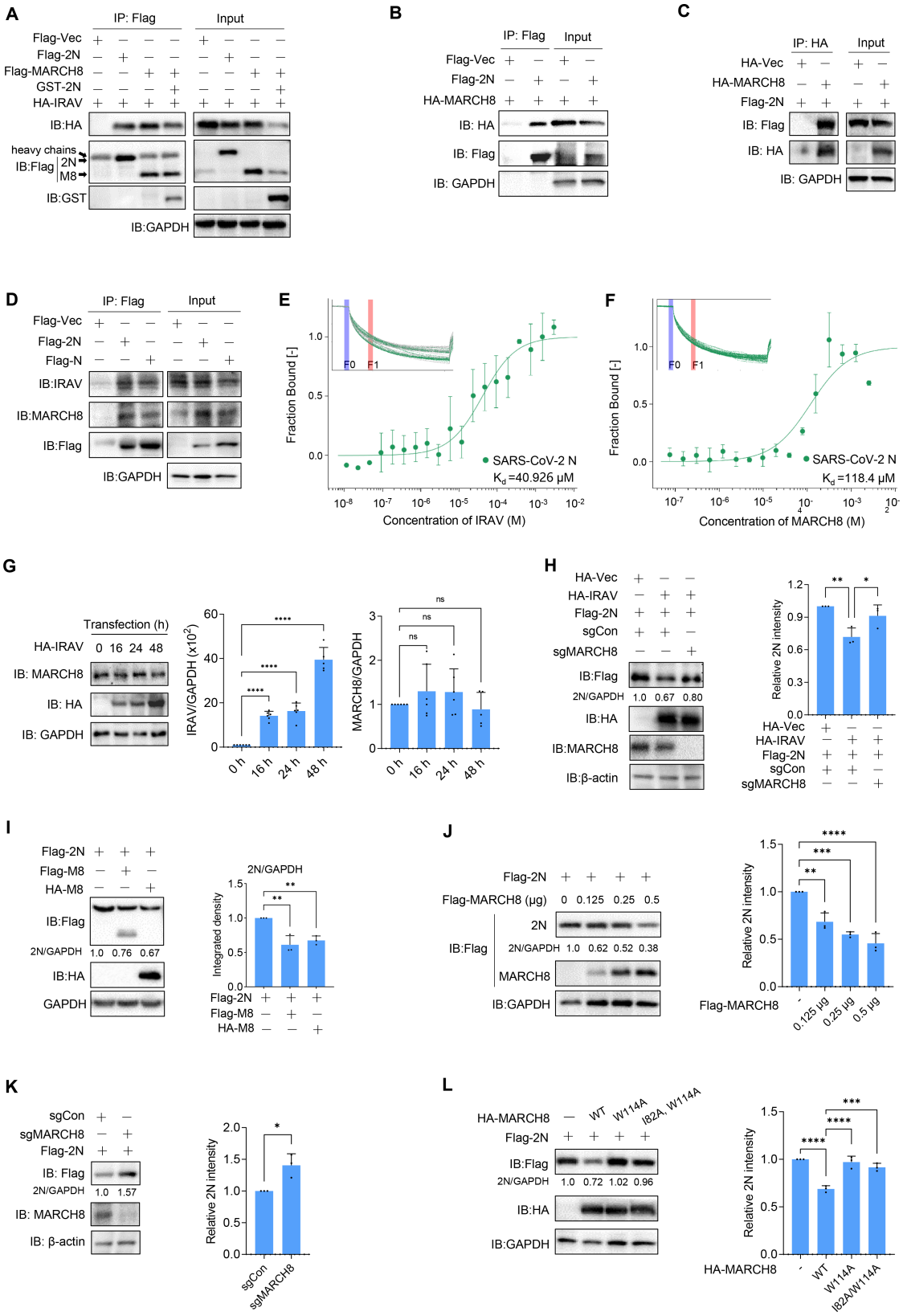

FIG 4 IRAV promotes 2N protein degradation through MARCH8. (A) HEK293T cells were co-transfected with the combinations of Flag-2N plus HA-IRAV, Flag-MARCH8 plus HA-IRAV, and Flag-MARCH8, HA-IRAV plus GST-2N. At 48 hpt, the presence of IRAV, MARCH8, and 2N was analyzed by immunoblots with anti-HA, Flag, and GST antibodies. (B) HEK293T cells were co-transfected with Flag-tagged 2N or vector, together with HA-MARCH8. At 48 hpt, co-IP was

(Continued on next page)

FIG 4 (Continued)

performed using the anti-Flag beads, and the immunocomplexes were analyzed by immunoblots. (C) HEK293T cells were co-transfected with HA-tagged MARCH8 or a vector together with Flag-2N. At 48 hpt, co-IP was performed using the anti-HA beads, and the immunocomplexes were analyzed by immunoblots. (D) HEK293T cells were transfected with Flag-tagged 2N, N, or vector. At 48 hpt, co-IP was performed using anti-Flag beads. The presence of endogenous IRAV and MARCH8 was analyzed by immunoblots. (E and F) The binding of fluorescently labeled SARS-CoV-2 N protein to IRAV (E) and MARCH8 (F) was measured by MST. (G) HEK293T cells were transfected with IRAV. At the indicated times, the expression of IRAV and MARCH8 was detected by immunoblots (left) and qPCR (right). (H) HEK293T cells transfected with sgMARCH8 or sgControl were cultured for 48 h, transfected with 2N and IRAV, and incubated for another 24 h. Cell lysates were analyzed by immunoblots. (I) HEK293T cells were co-transfected with 2N and Flag or HA-tagged MARCH8 (M8) plasmids. At 24 hpt, cells were lysed for immunoblots. (J) HEK293T cells were co-transfected with 2N and dose-escalated MARCH8 plasmids. At 24 hpt, cells were lysed for immunoblots. (K) HEK293T cells transfected with sgMARCH8 or sgControl were cultured for 48 h, transfected with 2N, and incubated for another 24 h, and cells were lysed for immunoblots. (L) HEK293T cells were co-transfected with Flag-2N plus HA-MARCH8 (WT, W114A mutant, W114A/I82A mutant) plasmids. At 24 hpt, cells were lysed for immunoblots. The gray-scale statistical analysis of three independent experiments was displayed on the right of (H) through (L).

lysosome after treatment with lysosome inhibitors CQ or BafA1 (Fig. 5C). Collectively, these results demonstrated that MARCH8 degraded SARS-CoV-2 N protein in a lysosome-dependent pathway.

As an E3 ubiquitin ligase, MARCH8 mediates protein ubiquitination and degradation. Indeed, SARS-CoV-2 N protein was ubiquitinated by MARCH8, while less ubiquitination was observed in MARCH8^{W114A} and MARCH8$^{I82A/W114A}$ mutants (Fig. 5D), demonstrating that MARCH8 induced the ubiquitination of 2N protein. We then determined the type of polyubiquitin linkage to 2N catalyzed by MARCH8 and found that only K48-ubiquitin promoted polyubiquitination of 2N (Fig. 5E). Based on recent studies, the substrate proteins that are ubiquitinated by MARCH8 are recognized by the cargo receptor NDP52/CALCOCO2, which delivers them to the autolysosome for degradation (27–30). To explore whether the cargo receptor for MARCH8-degraded 2N protein is NDP52, we performed co-IP assays. We observed that IRAV co-immunoprecipitated with both endogenous and exogenous NDP52 in HEK293T cells (Fig. 5F and G) and 2N interacted with both IRAV and NDP52 (Fig. 5H). According to immunofluorescence analysis, 2N was also co-localized with IRAV and NDP52 (Fig. 5I). These results demonstrated that NDP52 was the cargo receptor for MARCH8 responsible for the degradation of 2N protein.

MARCH8 targets K143 of SARS-CoV-2 N for polyubiquitination

To identify the potential ubiquitination residue of the 2N protein, we first mapped the potential domain targeted by EGR1 and MARCH8. SARS-CoV-2 N protein contains three domains: the N-terminal domain (NTD, 46–176 aa), the serine/arginine-rich linker region (182–247 aa), and the C-terminal domain (CTD, 247–364 aa) (31, 32). We constructed a series of plasmids expressing 2N protein domain truncations (Fig. 6A) (12). Full-length or truncated 2N proteins were co-transfected with EGR1 and MARCH8 plasmids into HEK293T cells. The immunoblotting results showed that only the N-arm combine NTD (N-NTD) domain of 2N protein was degraded by the ectopic expression of EGR1 and MARCH8 (Fig. 6B and C), demonstrating that EGR1 and MARCH8 targeted the N-terminal region of 2N protein for degradation. Moreover, the SPRY domain of TRIM25 reduced the expression of N-NTD domain truncation (Fig. 6D), further confirming that the N-terminal region of 2N was responsible for its degradation. In addition, we found that the N-NTD, CTD, and C-tail domains of the 2N protein all interacted with MARCH8 (Fig. 6E), which was consistent with our previous findings of the interaction of 2N domains and TRIM25 (12).

The N-NTD domain of the 2N protein has eight conserved lysine residues: K38, K61, K65, K100, K102, K127, K143, and K169, which are potential ubiquitination sites. Previous studies have shown that there are 16 lysine residues ubiquitinated in the 2N protein, of which K65, K100, K102, K143, and K169 are located in the N-NTD domain. The protein structure analysis highlights that the K338 ubiquitination located in the CTD domain is critical for 2N protein function (10). To explore the key lysine site for ubiquitination in 2N protein, we constructed five plasmids expressing the lysine mutants (K61R/K65R, K100R/K102R, K143R, K169R, and K338R/K342R) and co-transfected these 2N protein

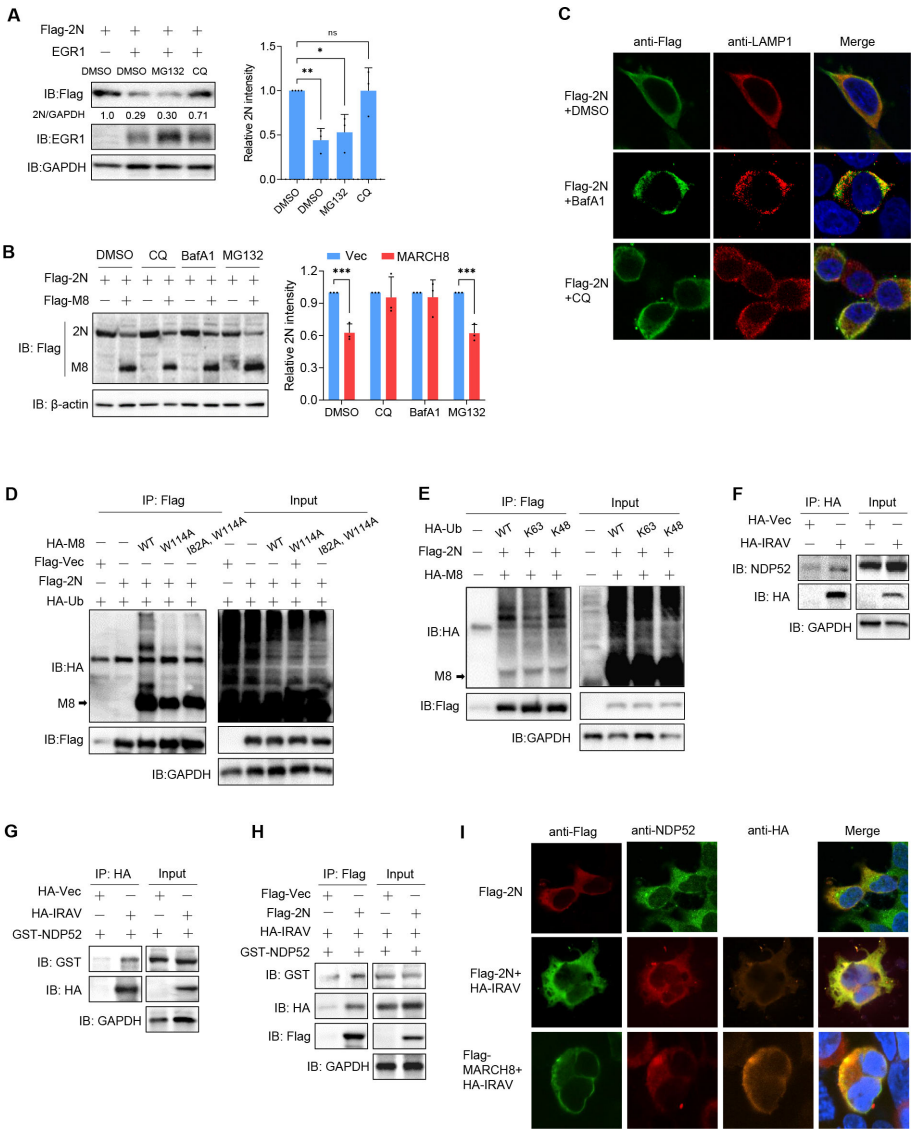

FIG 5 MARCH8 degrades 2N protein in a lysosome-dependent pathway. (A and B) HEK293T cells were co-transfected with 2N plus EGR1 (A) or MARCH8 (B) plasmids. At 24 hpt, cells were treated with DMSO, MG132, CQ, or BafA1 for another 6 h, followed by immunoblots using anti-Flag and EGR1 antibodies. (C) HEK293T cells were transfected with 2N plasmids. At 24 hpt, cells were treated with DMSO, BafA1, or CQ for another 6 h and subjected to immunofluorescence with anti-LAMP1 and Flag antibodies. Green: 2N signal; red: LAMP1 signal; blue: 4,6-diamino-2-phenyl indole (DAPI) (nuclei staining). Merge indicates the merged red, green, and blue channels. (D) HEK293T cells were co-transfected with HA-Ub and Flag-2N, together with HA-MARCH8 WT or mutant plasmids as indicated. At 24 hpt, cells were treated with the lysosome inhibitor CQ for another 6 h to avoid MARCH8-mediated degradation of 2N protein. The cell lysates were precipitated with anti-Flag beads, and the immunocomplexes were analyzed by immunoblots with anti-HA and Flag antibodies. (E) HEK293T cells were co-transfected with HA-MARCH8 and Flag-2N, together with HA-tagged WT Ub, lysine 63-linked ubiquitin chain (K63-UB), or lysine 48-linked ubiquitin chain (K48-UB). At 24 hpt, cells were treated with the lysosome inhibitor CQ for another 6 h and subjected to co-IP with anti-Flag beads. (F) HEK293T cells were transfected with HA-IRAV or vector. At 24 hpt, cells were subjected to co-IP with anti-HA beads. (G) HEK293T cells were transfected with GST-NDP52 and HA-IRAV or vector. At 24 hpt, cells were subjected to co-IP with anti-HA beads. (H) HEK293T cells were transfected with HA-IRAV, GST-NDP52, and Flag-2N as indicated. At 24 hpt, cells were treated with the lysosome inhibitor CQ for another 6 h to avoid IRAV-mediated degradation of 2N protein. The cells were subjected to co-IP with anti-Flag beads. (I) HEK293T cells were transfected with the indicated plasmids. At 24 hpt, cells were subjected to immunofluorescence with anti-NDP52, Flag, and HA antibodies. One- or two-way analysis of variance with multiple comparison correction was performed (*$P < 0.05$, **$P < 0.01$, and ***$P < 0.001$).

mutants combined with Ub and MARCH8 plasmids into HEK293T cells. The co-IP results showed that MARCH8 did not enhance the ubiquitination of the K143 mutant compared to wild-type (WT) and other mutants (Fig. 6F). Additionally, MARCH8 did not degrade the K143R mutant of the 2N protein (Fig. 6G). Taken together, our findings revealed that

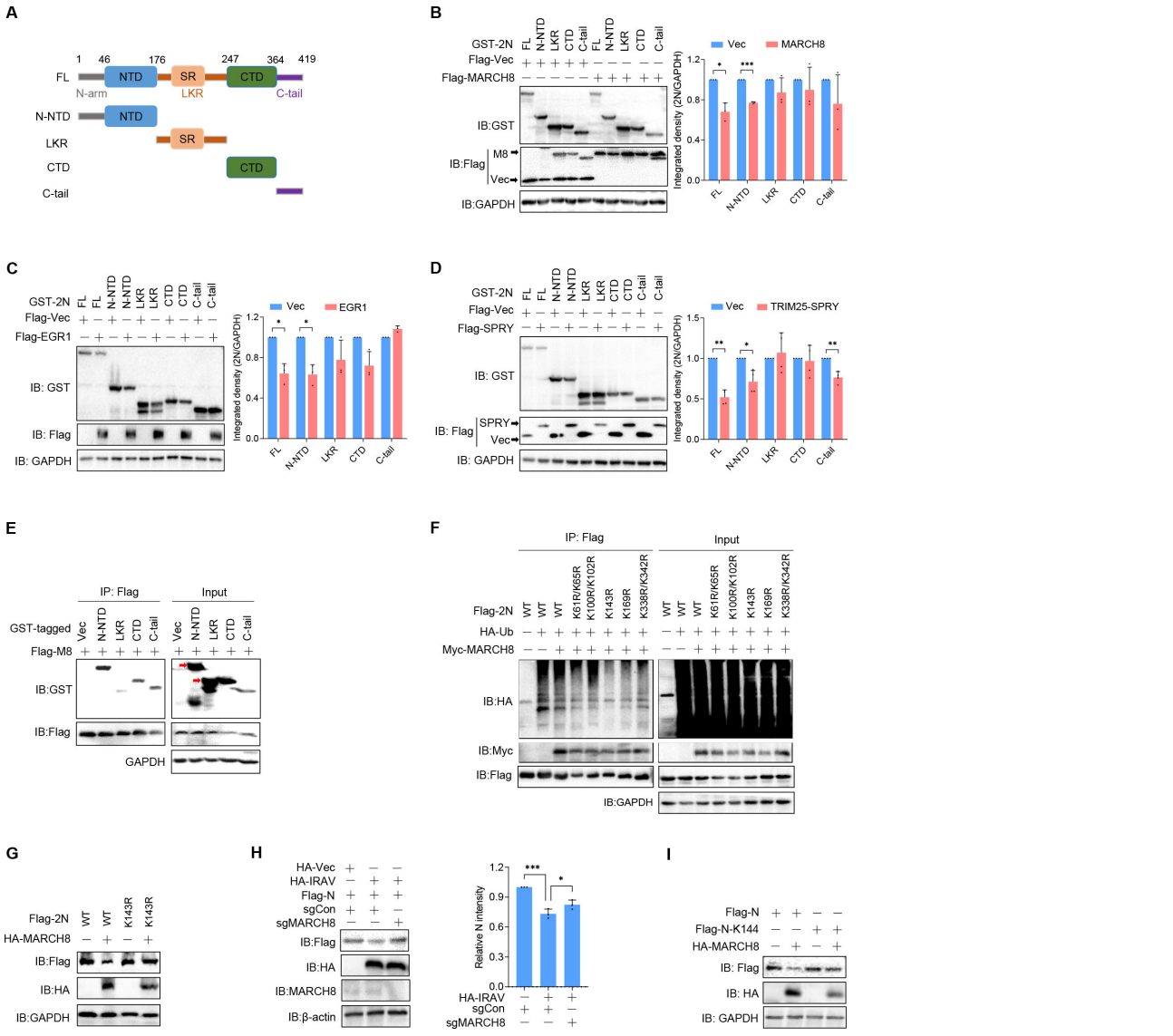

FIG 6 MARCH8 targets K143 of the 2N protein for polyubiquitination. (A) Domain mapping of the SARS-CoV-2 N protein. (B–D) HEK293T cells were co-transfected with the indicated GST-tagged truncations of 2N and Flag-tagged MARCH8 (B), Flag-tagged EGR1 (C), or Flag-SPRY (a domain of TRIM25) (D). At 24 hpt, cells were lysed for immunoblots. The gray-scale statistical analysis was displayed (right). (E) HEK293T cells were co-transfected with the indicated GST-tagged truncations of 2N protein and Flag-MARCH8 plasmids. At 24 hpt, cells were subjected to co-IP with anti-Flag beads, and the immunocomplexes were analyzed by immunoblots. The arrows indicate the target protein bands. (F) HEK293T cells were co-transfected with Flag-2N mutants, HA-Ub, and Myc-MARCH8 plasmids. At 24 hpt, cells were treated with lysosome inhibitor CQ for another 6 h and subjected to co-IP with anti-Flag beads. (G) HEK293T cells were co-transfected with HA-MARCH8 and Flag-2N WT or K143R mutant plasmids. At 24 hpt, cells were lysed for immunoblots. (H) HEK293T cells transfected with sgMARCH8 or sgControl were cultured for 48 h, transfected with N and IRAV, and incubated for another 24 h. Cell lysates were analyzed by immunoblots. The gray-scale statistical analysis was displayed (right). (I) HEK293T cells were co-transfected with HA-MARCH8 and Flag-N WT or K144R mutant plasmids. At 24 hpt, cells were lysed for immunoblots. A two-way analysis of variance with multiple comparison correction was performed (*P < 0.05, **P < 0.01, ***P < 0.001, and ****P < 0.0001).

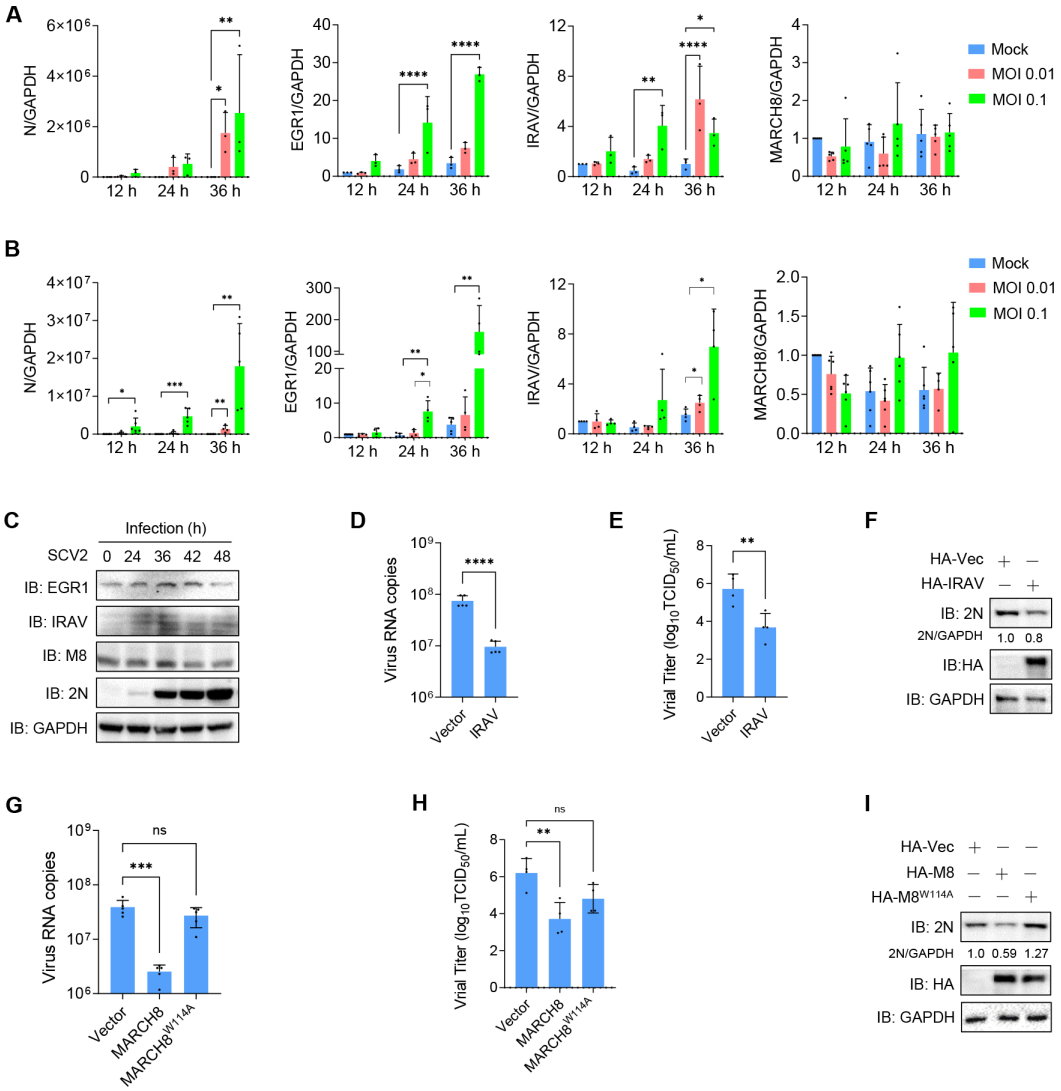

FIG 7 IRAV and MARCH8 inhibit SARS-CoV-2 replication. (A and B) Caco-2 cells (A) and HEK293T-ACE2 cells (B) were infected with SARS-CoV-2 at MOIs of 0.01 or 0.1. At 12, 24, and 36 hpi, the expression of viral N protein and host EGR1, IRAV, and MARCH8 genes was examined using qPCR. GAPDH was used as an internal reference control. (C) Caco-2 cells were infected with SARS-CoV-2 at an MOI of 0.01. Then, the cells were lysed for immunoblots with anti-EGR1, IRAV, MARCH8, and 2N antibodies at the indicated hours post infection. (D–F) Caco-2 cells were transfected with HA-IRAV or HA-vector. After 24 h, the cells were infected with SARS-CoV-2 at an MOI of 0.01. At 48 hpi, the viral RNA copies in supernatants were examined using qPCR (D); the viral titers were determined using $TCID_{50}$ assays (E); and the 2N and IRAV protein levels of cells were detected by immunoblots with anti-2N and HA antibodies (F). (G–I) Caco-2 cells were transfected with HA-vector and HA-MARCH8 WT or mutant plasmids. After 24 h, the cells were infected with SARS-CoV-2 at an MOI of 0.01. At 48 hpi, the viral RNA copies in the supernatant were examined using qPCR (G); the viral titers were examined using the $TCID_{50}$ assay (H); and the 2N and MARCH8 protein levels of cells were detected by immunoblots (I). A two-way analysis of variance with multiple comparison correction was performed (*P < 0.05, **P < 0.01, ***P < 0.001, and ****P < 0.0001).

MARCH8 targets K143, located in the N-NTD domain of the 2N protein, for ubiquitination and degradation.

We compared the N and 2N sequences and found that their N-NTD, especially K143, was conserved (Table S3). We further demonstrated that IRAV degraded N protein via MARCH8 (Fig. 6H) and the K144R mutant of N was no longer degraded by MARCH8 (Fig. 6I). These results suggest that SARS-CoV N has similar functions via a similar mechanism to 2N, which provides some insight regarding the conservative mechanism across different coronaviruses.

IRAV and MARCH8 inhibit SARS-CoV-2 replication

To verify the expression of EGR1, IRAV, and MARCH8 during virus infection, Caco-2 or HEK293T-ACE2 cells were infected with SARS-CoV-2. The timely expression showed that expression of EGR1 and IRAV was elevated at 24 and 36 h post infection (hpi), especially in the infection group with a multiple of infection (MOI) of 0.1, while MARCH8 was not affected (Fig. 7A and B). The protein levels of EGR1 and IRAV were also increased at 24 and 36 h after infection, whereas they decreased almost to the background level at 48 hpi (Fig. 7C). We further explored whether IRAV and MARCH8 inhibit SARS-CoV-2 replication. Caco-2 cells that expressed exogenous IRAV, MARCH8, or mutants were infected with SARS-CoV-2. At 48 hpi, SARS-CoV-2 replication levels were detected using qPCR, $TCID_{50}$, and immunoblots, indicating that IRAV and MARCH8 repressed virus replication and the $MARCH8^{W114A}$ mutant lost the ability to inhibit viral replication (Fig. 7D through I). These results demonstrated that EGR1 and IRAV are induced by SARS-CoV-2 infection and inhibit viral replication dependent on the ubiquitin ligase activity of MARCH8.

DISCUSSION

SARS-CoV-2 has developed multiple strategies to antagonize host IFN systems and inhibit host restriction factors (33, 34). The present study showed that SARS-CoV-2 N protein inhibited IFN-I responses by decreasing EGR1 expression and ectopic expression of EGR1 inhibited SARS-CoV-2 replication. Mechanistically, EGR1 encouraged IRAV expression, which could interact with 2N protein to mediate its degradation through the ubiquitin ligase MARCH8 in a lysosome-dependent pathway (Fig. 8) . We also demonstrated that SARS-CoV-2 infection induced the expression of EGR1 and IRAV but not MARCH8 and ectopic expression of both IRAV and MARCH8 suppressed SARS-CoV-2 replication.

EGR1 is induced by interferons and acts as a transcription factor to drive ISG expression (18, 20, 21). As positive feedback, EGR1 enhances IFN-I signaling by promoting phosphorylation of TBK1, thereby suppressing viral replication (18). The effect of EGR1 on SARS-CoV-2 infection is still controversial. The expression of EGR1 is increased in SARS-CoV-2-infected human lung-derived cells (A549-ACE2) (10), whereas it is reduced in SARS-CoV-2-infected epithelial cells (Calu-3) (36). Here, we found that SARS-CoV-2 infection induced EGR1 expression in both Caco-2 and HEK293T-ACE2 cells and the overexpression of EGR1 inhibited SARS-CoV-2 replication by degrading 2N protein, demonstrating that EGR1 functions as a new host restriction factor for SARS-CoV-2 to inhibit virus replication.

EGR1 has been shown to bind to the promoter of IRAV to facilitate IRAV expression, which recruits MARCH8 to inhibit PEDV replication (17). In the present study, we demonstrated that IRAV expression is induced by EGR1 and IRAV interacts with SARS-CoV-2 N protein to mediate its degradation through MARCH8, indicating that EGR1 is a new host restriction factor for SARS-CoV-2 to inhibit virus replication through the E3 ubiquitin ligase MARCH8. As a novel interferon-stimulated gene, IRAV, also termed C19orf66, SHFL, and RyDEN, is upregulated upon multiple virus infections and exerts antiviral effects (37–39). For instance, IRAV interacts with the host cytoplasmic poly-A binding protein and interferes with the replication complex formation to repress dengue virus replication (40, 41), impedes early gene expression of Kaposi's Sarcoma-associated herpesvirus (42), induces lysosome-dependent degradation of Zika virus NS3 protein (43), and alters the morphology of the replication organelle of hepatitis C virus (HCV) (44). In addition, as a trans-acting programmed −1 ribosomal frame shifting (−1PRF) inhibitor, IRAV exerts an antiviral effect through binding to viral −1PRF RNA and the translating ribosome to destroy −1PRF process (45–47). These studies suggest that IRAV may be a universal host restriction factor that inhibits virus infection. We will further verify whether IRAV suppresses SARS-CoV-2 replication through inhibiting the −1PRF process.

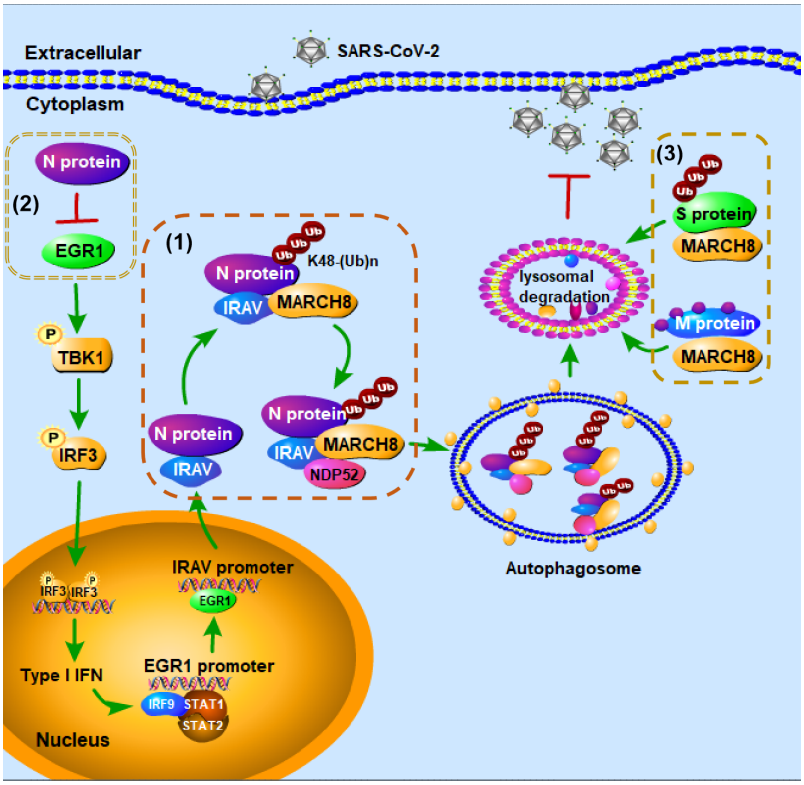

FIG 8 Schematic overview of the working model of the interactions between SARS-CoV-2 and host restriction factors EGR1 and MARCH8 (1). After SARS-CoV-2 invasion, EGR1 promotes expression of IRAV, which interacts with 2N protein and mediates its degradation through the ubiquitin ligase MARCH8 in a lysosome-dependent pathway (2). Simultaneously, the SARS-CoV-2 N protein inhibits the IFN-I response by suppressing EGR1 expression to obtain successful replication (3). MARCH8 mediates degradation of SARS-CoV-2 S and M glycoproteins to inhibit viral replication (22, 23, 35).

As a member of the MARCH E3 ubiquitin ligase family, MARCH8 not only degrades host transmembrane proteins to regulate cellular homeostasis but also acts as an antiviral factor to degrade viral envelope glycoproteins through ubiquitination-dependent or tyrosine motif-dependent pathways (22–25). The influenza A virus M2 protein can acquire non-lysine mutants at 78 or 79 positions to resist MARCH8-mediated ubiquitination and degradation, leading to the emergence of the human adaptive H1N1 IAV in 1977 (48). SARS-CoV-2 is a rapidly evolving virus. SARS-CoV-2 spike (S) and N proteins display a strong propensity for mutations (49–51), whose mutations are involved in modulating viral transmissibility, replication, and virulence (52–54). A number of studies have demonstrated that MARCH8 can degrade the SARS-CoV-2 S glycoprotein by different mechanisms (55). MARCH8 can trap the S protein on the cell surface into an intracellular LAMP-1$^+$ compartment for degradation (23), and MARCH8 can also recognize the cytoplasmic lysine residues of the S protein, resulting in its ubiquitination and lysosomal degradation (22). Additionally, MARCH8 degrades the heavily glycosylated form of SARS-CoV-2 M protein due to the colocalization of MARCH8 and the heavily glycosylated form of M protein at the Golgi complex (35). Here, we found that knockout of endogenous MARCH8 reversed IRAV-mediated 2N protein degradation and overexpression of MARCH8 inhibited SARS-CoV-2 replication, which indicated that MARCH8 is responsible for the inhibition of SARS-CoV-2 replication mediated by EGR1 and IRAV. Specifically, MARCH8 induced SARS-CoV-2 N protein degradation via catalyzing the K48-linked polyubiquitination at the lysine residue 143, suggesting that we should pay close attention to the K143 site of 2N protein, whose mutation may result in resistance to MARCH8.

In summary, our study demonstrated that the SARS-CoV-2 N protein inhibited IFN responses by reducing EGR1 expression. Additionally, the replication of SARS-CoV-2 was inhibited by EGR1 via the degradation of 2N protein. Mechanistically, EGR1 promoted expression of IRAV, which interacted with 2N and induced its degradation via the E3 ubiquitin ligase MARCH8 using the cargo receptor NDP52. Moreover, we found that IRAV degraded SARS-CoV N protein via MARCH8, indicating that the antiviral role of the EGR1-IRAV-MARCH8 signal axis may be conserved in the family Coronaviridae.

MATERIALS AND METHODS

Construction of SARS-CoV and SARS-CoV-2 N proteins in stably expressing cells

The full-length cDNAs of SARS-CoV and SARS-CoV-2 N proteins obtained from Flag-tagged expressing VR1012 plasmids (12) were inserted into lentiviral vectors to package lentivirus particles. HEK293T cells were infected with concentrated lentivirus particles and screened with puromycin to acquire N-protein-stably expressing cells, HEK293T-N and HEK293T-2N. HEK293T cells stably expressing Flag-tagged GFP were also constructed and used as a control.

Cell culture and virus infection

HEK293T, HEK293T-ACE2, Caco-2, Vero, and N proteins stable-expressing cells were grown and maintained in Dulbecco's modified Eagle's medium (DMEM) (catalog no. HY-VW-SH30022-LS; HyClone, Logan, UT, USA) containing 10% heat-inactivated fetal bovine serum (catalog no. E600001; BBI, Shanghai, China), 100 U/mL of ampicillin, and 100 µg/mL of streptomycin (catalog no. B540732; Sangon, Shanghai, China).

Virus infection was performed as previously described (12). Briefly, Caco-2 or HEK293T-ACE2 cells were infected with SARS-CoV-2 at an MOI of 0.01 or 0.1 (BetaCoV/wuhan/AMMS01/2020) (56), and the cells and supernatants were harvested to determine virus replication as previously described (57). The cell-culture supernatants were used to extract RNA using the QIAamp Viral RNA Mini Kit (QIAGEN, Germany). Detection of viral genomes was performed by qPCR using SARS-CoV-2-specific primers 5′-GGGGAACTTCTCCTGCTAGAAT-3′ (forward) and 5′-CAGACATTTTGCTCTCAAGCTG-3′ (reverse). The qPCR was performed using the HiScript II U^+ One Step qRT-PCR Probe Kit (Vazyme, China) in an ABI 7500 real-time PCR system (Applied Biosystem, USA), using the following cycling conditions: 50°C for 15 min, 95°C for 30 s, and 40 cycles of 95°C for 10 s, followed by 63°C for 35 s. Quantitative conversion of the virus copy number with the Ct value was obtained by the formula (copies)/µL = 10^[(Value of Ct − 45.949)/−3.29], which was generated by performing a standard curve with DNA derived from a viral N gene-expressing plasmid stock with a known plasmid concentration. Moreover, infected supernatants were assayed for infectious viral titers using the $TCID_{50}$ method. Briefly, Vero cells were seeded in 96-well plates at 20,000 cells per well. After 24 h, infectious supernatants were applied at 10-fold serial dilutions ranging from 10^{-1} to 10^{-6} and added to the well plate, and the viral cytopathogenic effect was detected by staining cells with crystal violet. The $TCID_{50}$ values were calculated via the Reed-Muench formula. All experiments infected with SARS-CoV-2 were conducted in the Biosafety Level 3 laboratory.

Antibodies and reagents

Antibodies against GST (catalog no. 10000-0-AP), Flag (catalog no. 66008-3-Ig or 20543-1-AP), HA (catalog no. 51064-2-AP or 66006-2-Ig), IRF9 (catalog no. 14167-1-AP), EGR1 (catalog no. 22008-1-AP), IFIT3 (catalog no. 15201-1-AP), IRAV (catalog no. 27865-1-AP), NDP52 (catalog no. 12229-1-AP), glyceraldehyde 3-phosphate dehydrogenase (GAPDH; catalog no. 60004-1-Ig or 10494-1-AP), and CoraLite 594-, 647-, or 488-conjugated IgG secondary antibodies (catalog no. SA0013-3, SA00013-2, and SA00013-1)

were obtained from Proteintech (Rosemont, IL, USA); anti-STAT2 antibody (catalog no. ab32367) was purchased from Abcam (Cambridge, MA, USA); anti-pSTAT2 antibody (catalog no. 3540916) was obtained from Sigma-Aldrich (St. Louis, MO, USA); anti-IFIT1 (catalog no. 14769S) antibody was purchased from Cell Signaling Technology (Danvers, MA, USA); MARCH8 antibody (catalog no. FNab05004) was purchased from FineTest (Wuhan Fine Biotech Co., Ltd., Hubei, China); anti-LAMP-1 antibody (catalog no. 328602) was obtained from BioLegend (San Diego, USA); and human anti-SARS-CoV-2 N protein antibody (catalog no. S209903) was purchased from ZENBIO (Chengdu, China).

BafA1 (catalog no. S7046), Z-VAD-FMK (catalog no. S7023), and 3-methyladenine (catalog no. S2767) were purchased from Selleck (Houston, TX, USA). MG132 (catalog no. S2767) and CQ (catalog no. PHR1258) were obtained from Sigma-Aldrich.

Plasmids and sgRNA

The promoter reporter plasmids (pIFN-β-Fluc or pISRE-Fluc) expressing the firefly luciferase and the internal reference reporter plasmid pGL4.74, expressing the Renilla luciferase, were described previously (58). The expression vectors of Flag- or GST-tagged SARS-CoV-2 N and truncations, Flag-tagged SARS-CoV N and SPRY, and GST-tagged RIG-IN were obtained as described previously (12). The expression vectors of HA-tagged WT-Ub, K48-Ub, and K63-Ub were constructed in the previous study (59). The EGR1 plasmid (catalog no. PPL00335-2a) with an unfused GFP tag was purchased from the Public Protein/Plasmid Library (PPL, Jiangsu, China). The expression constructs of GFP, EGR1, IRAV, NDP52, MARCH8 or mutants, SARS-CoV, and SARS-CoV-2 N mutants were cloned into the VR1012 vector with a Flag- or HA-tag. The EGR1 and MARCH8 knockdown plasmids, including pLenti-EGR1-sgRNA (catalog no. L00231) and pLenti-MARCHF8-sgRNA (catalog no. L09805), which simultaneously express Cas9, sgRNA of the target gene, and puromycin, were purchased from Beyotime Biotechnology (Shanghai, China). Transfection of plasmids into HEK293T or Caco-2 cells was performed using Lipofectamine 2000 (catalog no. 11668019; Invitrogen, San Diego, CA, USA).

RNA sequencing and analysis

SARS-CoV and SARS-CoV-2 N proteins stably expressing cells were transfected with or without poly(I:C) (catalog no. 61401; Cell Signaling Technology), and GFP-stably expressing cells were used as controls. At 24 hpt, cells were collected for RNA sequencing at Major Bio (Shanghai, China) (http://www.majorbio.com/), in which GPF/2 N/N were the stably expressing cells without poly(I:C) stimulation, and GPF_S /2N_S /N_S were the cells with poly(I:C) stimulation. The Deseq2 package in the R software was used to analyze DEGs between different groups with the criteria of |log (fold change)|>1 and $P < 0.05$. The PCA and heatmaps were generated with the R program. The Gene Ontology analysis was performed by DAVID. The top 10 enriched GO biological pathways for each group of DEGs were selected, resulting in 40 unique GO terms across all groups.

Quantitative real-time PCR

qPCR was performed using the primers in Table S4 as previously described (60). In brief, cells were washed twice with PBS and lysed using a lysis buffer. Total RNA was extracted using an EasyPure RNA Kit (catalog no. ER101; TransGen, China) according to the manufacturer's instructions. The extracted RNA was transcribed into cDNA using the cDNA Synthesis SuperMix (catalog no. AT341; TransGen), followed by qPCR with SYBR (Roche, Basel, Switzerland) using the Step-One Plus real-time PCR detection system (Applied Biosystems). The GAPDH gene was used as the reference gene for normalization.

Dual luciferase reporter assay

Cells were co-transfected with the indicated plasmids together with the luciferase reporter plasmids and lysed at 24 hpt. The firefly luciferase and Renilla luciferase activities were detected through the dual-luciferase reporter assay (catalog no. E1910; Promega, Madison, WI, USA) (61). The firefly luciferase activities were normalized and analyzed based on Renilla luciferase activity. Data were obtained from at least three independent experiments.

Immunoblotting and coimmunoprecipitation assays

Immunoblotting and co-IP analyses were conducted as previously described (12). In brief, cells were transfected with the indicated plasmids for 24 h and lysed for 30 min with the lysis buffer supplemented with protease and phosphatase inhibitor cocktail (catalog no. 78442; Thermo Scientific). The cell lysates were centrifuged at 12,000 × *g* for 10 min at 4°C and denatured for 10 min in 1× protein loading buffer. Then, proteins were separated by 10% sodium dodecyl sulfate-polyacrylamide gel electrophoresis and transferred onto polyvinylidene fluoride (PVDF) membranes (catalog no. IPVH00010; Millipore). The membranes were blocked with 5% non-fat powdered milk (catalog no. A600669; BBI) in PBS containing 0.2% Tween-20 (PBST) for 1 h at room temperature and incubated with appropriate primary antibodies (1:1,000) at 4°C overnight. The membranes were then washed with PBST and incubated with an HRP-conjugated secondary antibody (1:10,000) for 2 h at room temperature. Antibody-antigen complexes were visualized with chemiluminescence substrate. For co-IP, the lysates were centrifuged at 12,000 × *g* for 10 min at 4°C, and the supernatants were incubated with anti-Flag M2 Affinity Gel (catalog no. A2220; Sigma-Aldrich) or anti-HA Affinity Gel (catalog no. E6779; Millipore, Billerica, MA, USA) at 4°C overnight. The binding beads were washed with PBST five times and denatured in 1× protein loading buffer for 10 min. Finally, the immunocomplex proteins were analyzed using immunoblotting analysis.

Immunofluorescence

HEK293T or Caco-2 cells cultured on the 12 mm coverslips were transfected with the indicated plasmids or infected with SARS-CoV-2. After 24 hpi, the cells were washed once with PBST and fixed with 4% paraformaldehyde (catalog no. Top0382; Biotopped) for 30 min at room temperature. Next, the cells were permeated with 0.5% Triton X-100 (catalog no. 20107ES76; YEASEN) for 15 min. After washing twice with PBST, the cells were blocked in 1% bovine serum albumin (BSA) for 2 h and incubated with the primary antibody at 4°C overnight. After washing three times with PBST, the cells were stained with fluorescent dye-conjugated IgG secondary antibodies, and nuclei were stained with 4′,6-diamidino-2-phenylindole (catalog no. 40728ES03; YEASEN, Shanghai, China). Fluorescence images were obtained with a confocal microscope (FV3000; OLYMPUS) and analyzed using the ImageJ software.

Microscale thermophoresis assay

The affinity of the SARS-CoV-2 N protein (catalog no. PCN001; CRGEN Technologies) with the recombinant proteins IRAV and MARCH8 (catalog no. TP312344 and TP311771; OriGene Technologies) was calculated using Monolith NT. 115 (NanoTemper Technologies GmbH, Munich, Germany). Briefly, fluorescent labeling of SARS-CoV-2 N with His-tag was conducted with the RED-Tris-NTA Protein Labeling Kit (catalog no. MO-L018; NanoTemper). The candidate interacting IRAV and MARCH8 proteins with different concentrations were incubated with 50 nM labeled 2N protein at room temperature for 30 min in PBST buffer, and samples were loaded into NanoTemper hydrophilic-treated capillaries for affinity measurement. The data were analyzed using the NanoTemper analysis software.

Statistical analysis

Prism 9.0.2 (Graph Pad) was used for statistical analyses. Statistical significance was analyzed using one- or two-way analysis of variance, and significance indicated by asterisks is designated as follows: *$P < 0.05$, **$P < 0.01$, ***$P < 0.001$, and ****$P < 0.0001$.

ACKNOWLEDGMENTS

We thank Dr. Nan Zhang for collecting the RNA sequencing data and making these data's graphical visualization publicly available.

This work was supported by grants from the National Natural Science Foundation of China (grant numbers 81972873 and 82272327), the Pearl River Talent Plan in Guangdong Province of China (grant number 2019CX01N111), the Scientific and Technological Research Projects of Guangzhou (grant number 202103000008), the National Key Research and Development Program of China (grant number 2022YFC2601900), and the Medical Innovation Team Project of Jilin University (2022JBGS02).

We declare that we have no conflicts of interest.

AUTHOR AFFILIATIONS

[1]Department of Infectious Diseases and Center of Infectious Diseases and Pathogen Biology, Key Laboratory of Organ Regeneration and Transplantation of the Ministry of Education, State Key Laboratory for Diagnosis and Treatment of Severe Zoonotic Infectious Diseases, Key Laboratory for Zoonosis of the Ministry of Education, The First Hospital of Jilin University, Changchun, China
[2]College of Wildlife and Protected Area, Northeast Forestry University, Harbin, China
[3]Research Unit of Key Technologies for Prevention and Control of Virus Zoonoses, Chinese Academy of Medical Sciences, Changchun Veterinary Research Institute, Chinese Academy of Agricultural Sciences, Changchun, China
[4]Department of Pathogenbiology, The Key Laboratory of Zoonosis, Chinese Ministry of Education, College of Basic Medicine, Jilin University, Changchun, China
[5]School of Life Sciences and Engineering, Foshan University, Foshan, China
[6]Department of Pediatric Surgery, The First Hospital of Jilin University, Changchun, China
[7]Guangdong Key Laboratory of Animal Conservation and Resource Utilization, Institute of Zoology, Guangdong Academy of Sciences, Guangzhou, China

AUTHOR ORCIDs

Yinghua Zhao http://orcid.org/0000-0002-2938-4787
Guoqing Wang http://orcid.org/0000-0001-9326-3755
Quan Liu http://orcid.org/0000-0003-3411-3196

FUNDING

Funder	Grant(s)	Author(s)
MOST | National Natural Science Foundation of China (NSFC)	81972873	Yinghua Zhao
MOST | National Natural Science Foundation of China (NSFC)	82272327	Ze-Dong Wang
广东省人力资源和社会保障厅 | Guangdong Provincial Pearl River Talents Program (广东珠江人才计划)	2019CX01N111	Quan Liu
Scientific and Technological Research Projects of Guangzhou	202103000008	Quan Liu
MOST | National Key Research and Development Program of China (NKPs)	2022YFC2601900	Ze-Dong Wang

AUTHOR CONTRIBUTIONS

Yinghua Zhao, Project administration, Validation, Writing – original draft | Liyan Sui, Data curation, Methodology | Ping Wu, Data curation, Formal analysis | Letian Li, Methodology, Resources | Ze-Dong Wang, Conceptualization, Supervision | Zhengkai Wei, Validation, Visualization | Zhijun Hou, Project administration, Supervision | Kaiyu Zhang, Project administration, Visualization | Junqi Niu, Project administration, Supervision, Validation | Ningyi Jin, Conceptualization, Project administration | Chang Li, Project administration, Resources | Jixue Zhao, Project administration, Resources | Guoqing Wang, Project administration, Validation | Quan Liu, Conceptualization, Funding acquisition, Supervision, Writing – review and editing.

DATA AVAILABILITY

The RNA sequencing data for this article are available in the GEO repository with accession number GSE189706. The data supporting the conclusions of this article are included within the article and its additional files or available from the authors upon reasonable request.

ADDITIONAL FILES

The following material is available online.

Supplemental Material

Tables S1 to S4 (JVI01028-23-s0001.xls). Supplemental tables.

REFERENCES

1. Schultze JL, Aschenbrenner AC. 2021. COVID-19 and the human innate immune system. Cell 184:1671–1692. https://doi.org/10.1016/j.cell.2021.02.029
2. Heuberger J, Trimpert J, Vladimirova D, Goosmann C, Lin M, Schmuck R, Mollenkopf HJ, Brinkmann V, Tacke F, Osterrieder N, Sigal M. 2021. Epithelial response to IFN-γ promotes SARS-CoV-2 infection. EMBO Mol Med 13:e13191. https://doi.org/10.15252/emmm.202013191
3. Lee JS, Park S, Jeong HW, Ahn JY, Choi SJ, Lee H, Choi B, Nam SK, Sa M, Kwon JS, Jeong SJ, Lee HK, Park SH, Park SH, Choi JY, Kim SH, Jung I, Shin EC. 2020. Immunophenotyping of COVID-19 and influenza highlights the role of type I interferons in development of severe COVID-19. Sci Immunol 5:eabd1554. https://doi.org/10.1126/sciimmunol.abd1554
4. Wilk AJ, Rustagi A, Zhao NQ, Roque J, Martínez-Colón GJ, McKechnie JL, Ivison GT, Ranganath T, Vergara R, Hollis T, Simpson LJ, Grant P, Subramanian A, Rogers AJ, Blish CA. 2020. A single-cell atlas of the peripheral immune response in patients with severe COVID-19. Nat Med 26:1070–1076. https://doi.org/10.1038/s41591-020-0944-y
5. Liu Q, Wang H, Zhang H, Sui L, Li L, Xu W, Du S, Hao P, Jiang Y, Chen J, Qu X, Tian M, Zhao Y, Guo X, Wang X, Song W, Song G, Wei Z, Hou Z, Wang G, Sun M, Li X, Lu H, Zhuang X, Jin N, Zhao Y, Li C, Liao M. 2022. The global succinylation of SARS-CoV-2-infected host cells reveals drug targets. Proc Natl Acad Sci U S A 119:e2123065119. https://doi.org/10.1073/pnas.2123065119
6. Hengel H, Koszinowski UH, Conzelmann KK. 2005. Viruses know it all: new insights into IFN networks. Trends Immunol 26:396–401. https://doi.org/10.1016/j.it.2005.05.004
7. Schoggins JW. 2019. Interferon-stimulated genes: what do they all do Annu Rev Virol 6:567–584. https://doi.org/10.1146/annurev-virology-092818-015756
8. Carlson CR, Asfaha JB, Ghent CM, Howard CJ, Hartooni N, Safari M, Frankel AD, Morgan DO. 2020. Phosphoregulation of phase separation by the SARS-CoV-2 N protein suggests a biophysical basis for its dual functions. Mol Cell 80:1092–1103. https://doi.org/10.1016/j.molcel.2020.11.025
9. Cubuk J, Alston JJ, Incicco JJ, Singh S, Stuchell-Brereton MD, Ward MD, Zimmerman MI, Vithani N, Griffith D, Wagoner JA, Bowman GR, Hall KB, Soranno A, Holehouse AS. 2021. The SARS-CoV-2 nucleocapsid protein is dynamic, disordered, and phase separates with RNA. Nat Commun 12:1936. https://doi.org/10.1038/s41467-021-21953-3
10. Stukalov A, Girault V, Grass V, Karayel O, Bergant V, Urban C, Haas DA, Huang Y, Oubraham L, Wang A, Hamad MS, Piras A, Hansen FM, Tanzer MC, Paron I, Zinzula L, Engleitner T, Reinecke M, Lavacca TM, Ehmann R, Wölfel R, Jores J, Kuster B, Protzer U, Rad R, Ziebuhr J, Thiel V, Scaturro P, Mann M, Pichlmair A. 2021. Multilevel proteomics reveals host perturbations by SARS-CoV-2 and SARS-CoV. Nature 594:246–252. https://doi.org/10.1038/s41586-021-03493-4
11. Gordon DE, Jang GM, Bouhaddou M, Xu J, Obernier K, White KM, O'Meara MJ, Rezelj VV, Guo JZ, Swaney DL, Tummino TA, Hüttenhain R, Kaake RM, Richards AL, Tutuncuoglu B, Foussard H, Batra J, Haas K, Modak M, Kim M, Haas P, Polacco BJ, Braberg H, Fabius JM, Eckhardt M, Soucheray M, Bennett MJ, Cakir M, McGregor MJ, Li Q, Meyer B, Roesch F, Vallet T, Mac Kain A, Miorin L, Moreno E, Naing ZZC, Zhou Y, Peng S, Shi Y, Zhang Z, Shen W, Kirby IT, Melnyk JE, Chorba JS, Lou K, Dai SA, Barrio-Hernandez I, Memon D, Hernandez-Armenta C, Lyu J, Mathy CJP, Perica T, Pilla KB, Ganesan SJ, Saltzberg DJ, Rakesh R, Liu X, Rosenthal SB, Calviello L, Venkataramanan S, Liboy-Lugo J, Lin Y, Huang X-P, Liu Y, Wankowicz SA, Bohn M, Safari M, Ugur FS, Koh C, Savar NS, Tran QD, Shengjuler D, Fletcher SJ, O'Neal MC, Cai Y, Chang JCJ, Broadhurst DJ, Klippsten S, Sharp PP, Wenzell NA, Kuzuoglu-Ozturk D, Wang H-Y, Trenker R, Young JM, Cavero DA, Hiatt J, Roth TL, Rathore U, Subramanian A, Noack J, Hubert M, Stroud RM, Frankel AD, Rosenberg OS, Verba KA, Agard DA, Ott M, Emerman M, Jura N, von Zastrow M, Verdin E, Ashworth A, Schwartz O, d'Enfert C, Mukherjee S, Jacobson M, Malik HS, Fujimori DG, Ideker T, Craik CS, Floor SN, Fraser JS, Gross JD, Sali A, Roth BL, Ruggero D, Taunton J, Kortemme T, Beltrao P, Vignuzzi M, García-Sastre A, Shokat KM, Shoichet BK, Krogan NJ. 2020. A SARS-CoV-2 protein interaction map reveals targets for drug repurposing. Nature 583:459–468. https://doi.org/10.1038/s41586-020-2286-9
12. Zhao Y, Sui L, Wu P, Wang W, Wang Z, Yu Y, Hou Z, Tan G, Liu Q, Wang G. 2021. A dual-role of SARS-CoV-2 nucleocapsid protein in regulating innate immune response. Sig Transduct Target Ther 6:331. https://doi.org/10.1038/s41392-021-00742-w
13. Gómez-Martín D, Díaz-Zamudio M, Galindo-Campos M, Alcocer-Varela J. 2010. Early growth response transcription factors and the modulation of

immune response: implications towards autoimmunity. Autoimmun Rev 9:454–458. https://doi.org/10.1016/j.autrev.2009.12.006
14. Sukhatme VP. 1990. Early transcriptional events in cell growth: the EGR family. J Am Soc Nephrol 1:859–866. https://doi.org/10.1681/ASN.V16859
15. Buehler J, Carpenter E, Zeltzer S, Igarashi S, Rak M, Mikell I, Nelson JA, Goodrum F. 2019. Host signaling and EGR1 transcriptional control of human cytomegalovirus replication and latency. PLoS Pathog 15:e1008037. https://doi.org/10.1371/journal.ppat.1008037
16. Baer A, Lundberg L, Swales D, Waybright N, Pinkham C, Dinman JD, Jacobs JL, Kehn-Hall K. 2016. Venezuelan equine encephalitis virus induces apoptosis through the unfolded protein response activation of EGR1. J Virol 90:3558–3572. https://doi.org/10.1128/JVI.02827-15
17. Wang H, Kong N, Jiao Y, Dong S, Sun D, Chen X, Zheng H, Tong W, Yu H, Yu L, Zhang W, Tong G, Shan T. 2021. EGR1 suppresses porcine epidemic diarrhea virus replication by regulating IRAV to degrade viral nucleocapsid protein. J Virol 95:e0064521. https://doi.org/10.1128/JVI.00645-21
18. Zhu Z, Du X, Li P, Zhang X, Yang F, Cao W, Tian H, Zhang K, Liu X, Zheng H. 2018. Early growth response gene-1 suppresses foot-and-mouth disease virus replication by enhancing type I interferon pathway signal transduction. Front Microbiol 9:2326. https://doi.org/10.3389/fmicb.2018.02326
19. Rabaan AA, Al-Ahmed SH, Haque S, Sah R, Tiwari R, Malik YS, Dhama K, Yatoo MI, Bonilla-Aldana DK, Rodriguez-Morales AJ. 2020. SARS-CoV-2, SARS-CoV, and MERS-COV: a comparative overview. Infez Med 28:174–184.
20. Ramana CV, Gil MP, Han Y, Ransohoff RM, Schreiber RD, Stark GR. 2001. Stat1-independent regulation of gene expression in response to IFN-γ. Proc Natl Acad Sci U S A 98:6674–6679. https://doi.org/10.1073/pnas.111164198
21. Cao XM, Guy GR, Sukhatme VP, Tan YH. 1992. Regulation of the EGR-1 gene by tumor necrosis factor and interferons in primary human fibroblasts. J Biol Chem 267:1345–1349.
22. Zhang Y, Ozono S, Tada T, Tobiume M, Kameoka M, Kishigami S, Fujita H, Tokunaga K, Kalia M. 2022. MARCH8 targets cytoplasmic lysine residues of various viral envelope glycoproteins. Microbiol Spectr 10:e0061821. https://doi.org/10.1128/spectrum.00618-21
23. Lun CM, Waheed AA, Majadly A, Powell N, Freed EO. 2021. Mechanism of viral glycoprotein targeting by membrane-associated RING-CH proteins. mBio 12:e00219-21. https://doi.org/10.1128/mBio.00219-21
24. Umthong S, Lynch B, Timilsina U, Waxman B, Ivey EB, Stavrou S. 2021. Elucidating the antiviral mechanism of different MARCH factors. mBio 12:e03264-20. https://doi.org/10.1128/mBio.03264-20
25. Zhang Y, Tada T, Ozono S, Kishigami S, Fujita H, Tokunaga K. 2020. MARCH8 inhibits viral infection by two different mechanisms. Elife 9:e57763. https://doi.org/10.7554/eLife.57763
26. Stein JAC, Ianeselli A, Braun D. 2021. Kinetic microscale thermophoresis for simultaneous measurement of binding affinity and kinetics. Angew Chem Int Ed Engl 60:13988–13995. https://doi.org/10.1002/anie.202101261
27. Kong N, Shan T, Wang H, Jiao Y, Zuo Y, Li L, Tong W, Yu L, Jiang Y, Zhou Y, Li G, Gao F, Yu H, Zheng H, Tong G. 2020. BST2 suppresses porcine epidemic diarrhea virus replication by targeting and degrading virus nucleocapsid protein with selective autophagy. Autophagy 16:1737–1752. https://doi.org/10.1080/15548627.2019.1707487
28. Jiao Y, Kong N, Wang H, Sun D, Dong S, Chen X, Zheng H, Tong W, Yu H, Yu L, Huang Y, Wang H, Sui B, Zhao L, Liao Y, Zhang W, Tong G, Shan T. 2021. PABPC4 broadly inhibits Coronavirus replication by degrading nucleocapsid protein through selective autophagy. Microbiol Spectr 9:e0090821. https://doi.org/10.1128/Spectrum.00908-21
29. Dong S, Kong N, Wang C, Li Y, Sun D, Qin W, Zhai H, Zhai X, Yang X, Ye C, Ye M, Liu C, Yu L, Zheng H, Tong W, Yu H, Zhang W, Tong G, Shan T. 2022. FUBP3 degrades the porcine epidemic diarrhea virus nucleocapsid protein and induces the production of type I interferon. J Virol 96:e0061822. https://doi.org/10.1128/jvi.00618-22
30. Qin W, Kong N, Wang C, Dong S, Zhai H, Zhai X, Yang X, Ye C, Ye M, Tong W, Liu C, Yu L, Zheng H, Yu H, Lan D, Zhang W, Tong G, Shan T, Gallagher T. 2022. hnRNP K degrades viral nucleocapsid protein and induces type I IFN production to inhibit porcine epidemic diarrhea virus replication. J Virol 96. https://doi.org/10.1128/jvi.01555-22
31. Kang S, Yang M, Hong Z, Zhang L, Huang Z, Chen X, He S, Zhou Z, Zhou Z, Chen Q, Yan Y, Zhang C, Shan H, Chen S. 2020. Crystal structure of SARS-CoV-2 nucleocapsid protein RNA binding domain reveals potential unique drug targeting sites. Acta Pharm Sin B 10:1228–1238. https://doi.org/10.1016/j.apsb.2020.04.009
32. Zeng W, Liu G, Ma H, Zhao D, Yang Y, Liu M, Mohammed A, Zhao C, Yang Y, Xie J, Ding C, Ma X, Weng J, Gao Y, He H, Jin T. 2020. Biochemical characterization of SARS-CoV-2 nucleocapsid protein. Biochem Biophys Res Commun 527:618–623. https://doi.org/10.1016/j.bbrc.2020.04.136
33. Xia H, Cao Z, Xie X, Zhang X, Chen JY-C, Wang H, Menachery VD, Rajsbaum R, Shi P-Y. 2020. Evasion of type I interferon by SARS-CoV-2. Cell Rep 33:108234. https://doi.org/10.1016/j.celrep.2020.108234
34. Banerjee AK, Blanco MR, Bruce EA, Honson DD, Chen LM, Chow A, Bhat P, Ollikainen N, Quinodoz SA, Loney C, Thai J, Miller ZD, Lin AE, Schmidt MM, Stewart DG, Goldfarb D, De Lorenzo G, Rihn SJ, Voorhees RM, Botten JW, Majumdar D, Guttman M. 2020. SARS-CoV-2 disrupts splicing, translation, and protein trafficking to suppress host defenses. Cell 183:1325–1339. https://doi.org/10.1016/j.cell.2020.10.004
35. Umthong S, Lynch B, Timilsina U, Waxman B, Ivey EB, Stavrou S. 2021. Elucidating the antiviral mechanism of different MARCH factors. mBio 12:e03264-20. https://doi.org/10.1128/mBio.03264-20
36. Alexander MR, Brice AM, Jansen van Vuren P, Rootes CL, Tribolet L, Cowled C, Bean AGD, Stewart CR. 2021. Ribosome-profiling reveals restricted post transcriptional expression of antiviral cytokines and transcription factors during SARS-CoV-2 infection. Int J Mol Sci 22:3392. https://doi.org/10.3390/ijms22073392
37. Gaucher D, Therrien R, Kettaf N, Angermann BR, Boucher G, Filali-Mouhim A, Moser JM, Mehta RS, Drake DR III, Castro E, Akondy R, Rinfret A, Yassine-Diab B, Said EA, Chouikh Y, Cameron MJ, Clum R, Kelvin D, Somogyi R, Greller LD, Balderas RS, Wilkinson P, Pantaleo G, Tartaglia J, Haddad EK, Sékaly R-P. 2008. Yellow fever vaccine induces integrated multilineage and polyfunctional immune responses. J Exp Med 205:3119–3131. https://doi.org/10.1084/jem.20082292
38. Wang J, Nikrad MP, Phang T, Gao B, Alford T, Ito Y, Edeen K, Travanty EA, Kosmider B, Hartshorn K, Mason RJ. 2011. Innate immune response to influenza A virus in differentiated human alveolar type II cells. Am J Respir Cell Mol Biol 45:582–591. https://doi.org/10.1165/rcmb.2010-0108OC
39. Kash JC, Mühlberger E, Carter V, Grosch M, Perwitasari O, Proll SC, Thomas MJ, Weber F, Klenk HD, Katze MG. 2006. Global suppression of the host antiviral response by Ebola- and Marburgviruses: increased antagonism of the type I interferon response is associated with enhanced virulence. J Virol 80:3009–3020. https://doi.org/10.1128/JVI.80.6.3009-3020.2006
40. Suzuki Y, Chin W-X, Han Q, Ichiyama K, Lee CH, Eyo ZW, Ebina H, Takahashi H, Takahashi C, Tan BH, Hishiki T, Ohba K, Matsuyama T, Koyanagi Y, Tan Y-J, Sawasaki T, Chu JJH, Vasudevan SG, Sano K, Yamamoto N, Rice CM. 2016. Characterization of RyDEN (C19orf66) as an interferon-stimulated cellular inhibitor against dengue virus replication. PLoS Pathog 12:e1005357. https://doi.org/10.1371/journal.ppat.1005357
41. Balinsky CA, Schmeisser H, Wells AI, Ganesan S, Jin T, Singh K, Zoon KC. 2017. IRAV (FLJ11286), an interferon-stimulated gene with antiviral activity against dengue virus, interacts with MOV10. J Virol 91:e01606-16. https://doi.org/10.1128/JVI.01606-16
42. Rodriguez W, Srivastav K, Muller M. 2019. C19orf66 broadly escapes virus-induced endonuclease cleavage and restricts kaposi's sarcoma-associated herpesvirus. J Virol 93:e00373-19. https://doi.org/10.1128/JVI.00373-19
43. Wu Y, Yang X, Yao Z, Dong X, Zhang D, Hu Y, Zhang S, Lin J, Chen J, An S, Ye H, Zhang S, Qiu Z, He Z, Huang M, Wei G, Zhu X, Aguilar PV. 2020. C19orf66 interrupts Zika virus replication by inducing lysosomal degradation of viral NS3. PLoS Negl Trop Dis 14:e0008083. https://doi.org/10.1371/journal.pntd.0008083
44. Kinast V, Plociennikowska A, AnggakusumaT, Todt D, Brown RJP, Boldanova T, Zhang Y, Brüggemann Y, Friesland M, Engelmann M, Vieyres G, Broering R, Vondran FWR, Heim MH, Sitek B, Bartenschlager R, Pietschmann T, Steinmann E. 2020. C19orf66 is an interferon-induced inhibitor of HCV replication that restricts formation of the viral replication organelle. J Hepatol 73:549–558. https://doi.org/10.1016/j.jhep.2020.03.047

45. Wang X, Xuan Y, Han Y, Ding X, Ye K, Yang F, Gao P, Goff SP, Gao G. 2019. Regulation of HIV-1 Gag-Pol expression by shiftless, an inhibitor of programmed -1 ribosomal frameshifting. Cell 176:625–635. https://doi.org/10.1016/j.cell.2018.12.030
46. Yu D, Zhao Y, Pan J, Yang X, Liang Z, Xie S, Cao R. 2021. C19orf66 inhibits Japanese encephalitis virus replication by targeting -1 PRF and the NS3 protein. Virol Sin 36:1443–1455. https://doi.org/10.1007/s12250-021-00423-6
47. Hanners NW, Mar KB, Boys IN, Eitson JL, De La Cruz-Rivera PC, Richardson RB, Fan W, Wight-Carter M, Schoggins JW. 2021. Shiftless inhibits flavivirus replication *in vitro* and is neuroprotective in a mouse model of Zika virus pathogenesis. Proc Natl Acad Sci U S A 118:e2111266118. https://doi.org/10.1073/pnas.2111266118
48. Liu X, Xu F, Ren L, Zhao F, Huang Y, Wei L, Wang Y, Wang C, Fan Z, Mei S, Song J, Zhao Z, Cen S, Liang C, Wang J, Guo F. 2021. MARCH8 inhibits influenza A virus infection by targeting viral M2 protein for ubiquitination-dependent degradation in lysosomes. Nat Commun 12:4427. https://doi.org/10.1038/s41467-021-24724-2
49. Islam MR, Hoque MN, Rahman MS, Alam ASMRU, Akther M, Puspo JA, Akter S, Sultana M, Crandall KA, Hossain MA. 2020. Genome-wide analysis of SARS-CoV-2 virus strains circulating worldwide implicates heterogeneity. Sci Rep 10:14004. https://doi.org/10.1038/s41598-020-70812-6
50. Plante JA, Mitchell BM, Plante KS, Debbink K, Weaver SC, Menachery VD. 2021. The variant gambit: COVID-19's next move. Cell Host Microbe 29:508–515. https://doi.org/10.1016/j.chom.2021.02.020
51. Rahman MS, Islam MR, Alam ASMRU, Islam I, Hoque MN, Akter S, Rahaman MM, Sultana M, Hossain MA. 2021. Evolutionary dynamics of SARS-CoV-2 nucleocapsid protein and its consequences. J Med Virol 93:2177–2195. https://doi.org/10.1002/jmv.26626
52. Pachetti M, Marini B, Benedetti F, Giudici F, Mauro E, Storici P, Masciovecchio C, Angeletti S, Ciccozzi M, Gallo RC, Zella D, Ippodrino R. 2020. Emerging SARS-CoV-2 mutation hot spots include a novel RNA-dependent-RNA polymerase variant. J Transl Med 18:179. https://doi.org/10.1186/s12967-020-02344-6
53. Wu H, Xing N, Meng K, Fu B, Xue W, Dong P, Tang W, Xiao Y, Liu G, Luo H, Zhu W, Lin X, Meng G, Zhu Z. 2021. Nucleocapsid mutations R203K/G204R increase the infectivity, fitness, and virulence of SARS-CoV-2. Cell Host Microbe 29:1788–1801. https://doi.org/10.1016/j.chom.2021.11.005
54. Zhang L, Jackson CB, Mou H, Ojha A, Peng H, Quinlan BD, Rangarajan ES, Pan A, Vanderheiden A, Suthar MS, Li W, Izard T, Rader C, Farzan M, Choe H. 2020. SARS-CoV-2 spike-protein D614G mutation increases virion spike density and infectivity. Nat Commun 11:6013. https://doi.org/10.1038/s41467-020-19808-4
55. Yu C, Wang G, Liu Q, Zhai J, Xue M, Li Q, Xian Y, Zheng C. 2023. Host antiviral factors hijack furin to block SARS-CoV-2, ebola virus, and HIV-1 glycoproteins cleavage. Emerg Microbes Infect 12:2164742. https://doi.org/10.1080/22221751.2022.2164742
56. Zhang NN, Li XF, Deng YQ, Zhao H, Huang YJ, Yang G, Huang WJ, Gao P, Zhou C, Zhang RR, Guo Y, Sun SH, Fan H, Zu SL, Chen Q, He Q, Cao TS, Huang XY, Qiu HY, Nie JH, Jiang Y, Yan HY, Ye Q, Zhong X, Xue XL, Zha ZY, Zhou D, Yang X, Wang YC, Ying B, Qin CF. 2020. A thermostable mRNA vaccine against COVID-19. Cell 182:1271–1283. https://doi.org/10.1016/j.cell.2020.07.024
57. Shang C, Zhuang X, Zhang H, Li Y, Zhu Y, Lu J, Ge C, Cong J, Li T, Tian M, Jin N, Li X. 2021. Inhibitors of endosomal acidification suppress SARS-CoV-2 replication and relieve viral pneumonia in hACE2 transgenic mice. Virol J 18:46. https://doi.org/10.1186/s12985-021-01515-1
58. Tan G, Xiao Q, Song H, Ma F, Xu F, Peng D, Li N, Wang X, Niu J, Gao P, Qin FX-F, Cheng G. 2018. Type I IFN augments IL-27-dependent TRIM25 expression to inhibit HBV replication. Cell Mol Immunol 15:272–281. https://doi.org/10.1038/cmi.2016.67
59. Tan G, Yi Z, Song H, Xu F, Li F, Aliyari R, Zhang H, Du P, Ding Y, Niu J, Wang X, Su L, Qin FX-F, Cheng G. 2019. Type-I-IFN-stimulated gene TRIM5γ inhibits HBV replication by promoting HBx degradation. Cell Rep 29:3551–3563. https://doi.org/10.1016/j.celrep.2019.11.041
60. Sui L, Zhao Y, Wang W, Wu P, Wang Z, Yu Y, Hou Z, Tan G, Liu Q. 2021. SARS-CoV-2 membrane protein inhibits type I interferon production through ubiquitin-mediated degradation of TBK1. Front Immunol 12:662989. https://doi.org/10.3389/fimmu.2021.662989
61. Zhao Y, Chu X, Chen J, Wang Y, Gao S, Jiang Y, Zhu X, Tan G, Zhao W, Yi H, Xu H, Ma X, Lu Y, Yi Q, Wang S. 2016. Dectin-1-activated dendritic cells trigger potent antitumour immunity through the induction of TH9 cells. Nat Commun 7:12368. https://doi.org/10.1038/ncomms12368